



## Original Articles

## Radiation-induced glioblastoma stem cell-mediated T cell exhaustion via EGR1-Gal3-LAG3 axis in glioblastoma

Hui Huang<sup>a,1</sup>, Chenhua Li<sup>a,1</sup>, Hao You<sup>b,c,1</sup>, Zhen Zhang<sup>a</sup>, Qiankun Lin<sup>b,c</sup>, Junlei Yang<sup>b,c</sup>, Hang Yu<sup>b,c</sup>, Zhiting Li<sup>b,c</sup>, Gaoyuan Cui<sup>b,c</sup>, Kefan Song<sup>b,c,d</sup>, Qian Zhang<sup>b,c</sup>, Yun Chen<sup>a,e</sup>, Xiuxing Wang<sup>a,b,c,d</sup>, Junxia Zhang<sup>c,d,\*</sup>, Danling Gu<sup>a,b,c,\*\*</sup>, Chao Cheng<sup>a,\*\*\*</sup>, Junfei Shao<sup>a,\*\*\*\*</sup>

<sup>a</sup> The Affiliated Wuxi People's Hospital of Nanjing Medical University, Wuxi People's Hospital, Wuxi Medical Center, Nanjing Medical University, Wuxi, Jiangsu, 214000, China

<sup>b</sup> National Health Commission Key Laboratory of Antibody Techniques, Department of Cell Biology, Jiangsu Provincial Key Laboratory of Human Functional Genomics, School of Basic Medical Sciences, Nanjing Medical University, Nanjing, Jiangsu, 211166, China

<sup>c</sup> Institute for Brain Tumors, Jiangsu Key Lab of Cancer Biomarkers, Prevention and Treatment, Collaborative Innovation Center for Cancer Personalized Medicine, Nanjing Medical University, Nanjing, Jiangsu, 210029, China

<sup>d</sup> Department of Neurosurgery, The First Affiliated Hospital of Nanjing Medical University, Nanjing, Jiangsu, 210029, China

<sup>e</sup> Department of Immunology, School of Basic Medical Sciences, Nanjing Medical University, Nanjing, Jiangsu, 211166, China

## ARTICLE INFO

## Keywords:

LAG3  
Gal3  
Glioblastomas  
Glioblastoma stem cells  
T cell exhaustion

## ABSTRACT

Glioblastoma (GBM), a highly aggressive brain tumor, inevitably recurs due to therapy-resistant glioblastoma stem cells (GSCs). Lymphocyte activation gene 3 (LAG3), an inhibitory immune checkpoint, contributes to T cell exhaustion and facilitates tumor immune escape. Here, we investigate the evolution of GSC-T cell interaction and the functional status of GBM-infiltrating T cells following radiotherapy. Using single-cell RNA sequencing analysis, we identified that T cells from recurrent GBM patients exhibited more exhausted status than those in newly diagnosed GBM patients. We identified LAG3 as a key factor driving T cell exhaustion in recurrent GBM. Furthermore, radiation exposure induced the expression of galectin-3 (Gal3), a canonical ligand of LAG3. EGR1 transcriptionally upregulated Gal3 expression in irradiated GSCs, impairing cytotoxic activity of both CD4<sup>+</sup> and CD8<sup>+</sup> T-cell. The small molecule inhibitor targeting EGR1 in combination with anti-LAG3 blockade suppressed irradiated GBM tumor growth and extended the survival of orthotopic xenograft-bearing mice. Gal3 secreted by GSCs plays critical roles in maintaining T cell exhaustion, highlighting a radio-induced interplay between GSCs and GBM-infiltrating T cells. Targeting upstream regulator EGR1 and LAG3 informs a promising treatment strategy for GBM.

\*\*\*\* Corresponding author.

\*\*\* Corresponding author.

\*\* Corresponding author. The Affiliated Wuxi People's Hospital of Nanjing Medical University, Wuxi People's Hospital, Wuxi Medical Center, National Health Commission Key Laboratory of Antibody Techniques, Department of Cell Biology, Jiangsu Provincial Key Laboratory of Human Functional Genomics, School of Basic Medical Sciences, Institute for Brain Tumors, Jiangsu Key Lab of Cancer Biomarkers, Prevention and Treatment, Collaborative Innovation Center for Cancer Personalized Medicine, Nanjing Medical University, Nanjing, Jiangsu, 210029, China.

\* Corresponding authors. Institute for Brain Tumors, Jiangsu Key Lab of Cancer Biomarkers, Prevention and Treatment, Collaborative Innovation Center for Cancer Personalized Medicine, Department of Neurosurgery, The First Affiliated Hospital of Nanjing Medical University, Nanjing Medical University, Nanjing, Jiangsu, 210029, China.

E-mail addresses: [zjx232@njmu.edu.cn](mailto:zjx232@njmu.edu.cn) (J. Zhang), [gudanling@njmu.edu.cn](mailto:gudanling@njmu.edu.cn) (D. Gu), [Mr\\_chengchao@njmu.edu.cn](mailto:Mr_chengchao@njmu.edu.cn) (C. Cheng), [wxbrainscience@163.com](mailto:wxbrainscience@163.com) (J. Shao).

<sup>1</sup> These authors contributed equally: Hui Huang, Chenhua Li, Hao You.

<https://doi.org/10.1016/j.canlet.2025.218125>

Received 15 May 2025; Received in revised form 23 September 2025; Accepted 7 November 2025

Available online 8 November 2025

0304-3835/© 2025 Elsevier B.V. All rights reserved, including those for text and data mining, AI training, and similar technologies.

## 1. Introduction

Glioblastoma (GBM) represents one of the most aggressive primary brain neoplasms, characterized by uniformly poor prognosis and an inexorably devastating clinical course [1,2]. Despite aggressive multimodal therapy comprising maximal safe resection, radiotherapy, and adjuvant chemotherapy with temozolomide (TMZ), the median overall survival for GBM patients remains less than 16 months, with virtually inevitable tumor recurrence [3–6]. Glioblastoma stem cells (GSCs) exhibit core stem-like properties including self-renewal, multi-potency, and tumor maintenance [7–9]. Meanwhile, GSCs are thought to be therapy-resistant and therefore lead to tumor recurrence post-treatment [10,11].

GSCs live in a niche that consists of astrocytes, microglia, endothelial cells, tumor-associated macrophages (TAMs), and T cells [12]. The interactions between GSCs and T cells facilitate immunosuppression through two principal mechanisms [13,14]: (i) evasion of immune-mediated elimination by impairing cytotoxic T-cell priming [15], and (ii) active suppression of antitumor immunity via secretion of immunosuppressive cytokines [10,11], creating a permissive niche that drives malignant progression.

Accumulating evidence indicates that the heterogeneity and functional states of tumor-infiltrating T cells play pivotal roles in shaping antitumor immunity and the response to immunotherapy [16–18]. Chronic antigen exposure and sustained tumor-T cell crosstalk triggers a progressive loss of effector T-cell function, culminating in exhaustion characterized by elevated expression of co-inhibitory receptors (immune checkpoints) and concurrent impairment of cytokine secretion and clonal expansion capacities [19,20]. Although immune checkpoint blockade (ICB) therapy has achieved remarkable benefits in several cancers, its efficacy in GBM remains limited [21–24]. This disparity likely arises from GBM-intrinsic oncogenic properties and unique exhaustion status of recurrent GBM-infiltrating T cells [25–27]. The specific characteristics of T cell exhaustion and the mechanisms by which GSC-mediated immunosuppression in recurrent GBM remain to be explored.

Here, we performed single-cell transcriptomic profiling of newly diagnosed and recurrent GBM specimens, revealing a significantly elevated T cell exhaustion in recurrent tumors, which was correlated with the expression of inhibitory immune checkpoint—lymphocyte activation gene 3 (LAG3) [28]. Notably, radiation-induced upregulation of galectin 3 (Gal3) on GSCs—a ligand for LAG3—emerged as a key mediator of T cell dysfunction and GSC radioresistance, mediated through early growth response 1 (EGR1)-dependent transcriptional activation. These findings support a novel combined therapy incorporating EGR1 inhibition (ML264) and LAG3 blockade (relatlimab) to potentiate antitumor immunity and improve outcomes in GBM.

## 2. Materials and methods

### 2.1. Data collection

Gene expression data were acquired via GlioVis (<https://gliovis.shinyapps.io/GlioVis/>). Single-cell RNA sequencing (scRNA-seq) data were obtained from two publicly accessible datasets (GSE182109 and GSE163120) on the Gene Expression Omnibus (GEO) database (<http://www.ncbi.nlm.nih.gov/geo/>). The GSE182109 comprised 37 tumor specimens from 15 IDH-wildtype GBM patients (11 newly diagnosed GBM and 4 recurrent GBM). GSE163120 included 12 tumors specimens from 12 IDH-wildtype GBM patients (7 newly diagnosed GBM and 5 recurrent GBM). Gene sets for Gene Set Enrichment Analysis (GSEA) were from the Molecular Signatures Database (<https://www.gsea-msigdb.org/gsea/>).

### 2.2. Patients and human tumor samples

Paraffin-embedded and fresh tumor samples were obtained from patients with GBM who received surgical resection, from the department of neurosurgery, the First Affiliated Hospital of Nanjing Medical University. All samples were collected from patients who gave informed consent, and all related procedures were performed with the approval of the internal review and ethics boards of the First Affiliated Hospital of Nanjing Medical University (2021-SR-076).

### 2.3. Single-cell RNA sequencing data processing

Raw single-cell RNA-seq data were processed using Seurat v4.3.1 for quality control, retaining cells with >200 detected genes and <20 % mitochondrial reads, and excluding genes expressed in fewer than 3 cells. Log-normalization was performed with a scale factor of 10,000, followed by Harmony v0.1.1 to correct batch effects across samples. Dimensionality reduction was carried out using principal component analysis (PCA), and the first 20 principal components (PCs) were selected based on elbow plot inspection and JackStraw resampling tests. Uniform Manifold Approximation and Projection (UMAP) was used for visualization, and clustering was performed using the Louvain algorithm with a resolution parameter of 0.5, optimized to yield biologically interpretable clusters. Cell-type annotation was performed by manual curation of cluster-specific marker expression and confirmed by cluster-wise differential expression analysis (Seurat FindAllMarkers). Cluster identities were assigned using canonical markers as follows: B cells (CD79A, CD79B, MS4A1, IGHG1, IGHG3); T cells (CD3D, CD3E, CD8A, CD8B); Myeloid cells (CD68, FCGR3A, CD14, CSF1R, C1QA); Tumor cells (SOX2, OLIG1, OLIG2, GFAP, S100B); Pericytes (ACA2, PDGFRB); Oligodendrocytes (ALCAM, MBP). Gene expression patterns of LGALS3 and LAG3 were visualized using Seurat's FeaturePlot function and refined with ggplot2 v3.5.0.

### 2.4. T cell exhaustion (TEX) analysis

T cell exhaustion status was evaluated through computational scoring of a TEX gene signature [29] (HLA-A, HLA-B, B2M, JAK1, STAT6, PDGFRB, IRF1, MET, RBM10, NFKBIE, PRKD2, EML4, LTB, LOX, WAS, PRF1, DDB2, IL7R, LATS2, CDH11, MYH11, CD79B, CBL, ZEB1, CCR7, P2RY8, KZF3, BTK, MSI2, TCF4, ERG, PCDH17, SFMBT2, IRF4, SP140, ZNF521, AXIN2, TLL1, CR1, DCC). The AddModuleScore function in Seurat (v4.3.1) was employed to calculate individual T cell exhaustion scores, with resultant values projected onto UMAP embeddings for spatial evaluation. Comparative analysis of TEX scores was performed across identified T cell subclusters to assess exhaustion state heterogeneity. The TEX signature expression patterns were further validated through violin plot visualization with ggplot2 v3.5.0.

### 2.5. Immunohistochemistry (IHC)

All slides were first deparaffinized in xylene and rehydrated, followed by washing for 3 times using PBS. Slides were then incubated in goat serum dilution buffer (GSDB) for 1 h in a wet chamber at room temperature. The slides were incubated with primary antibody diluted in GSDB overnight at 4 °C in a wet chamber. Primary antibody used is as follows: LAG-3/CD223 Polyclonal Antibody, Proteintech, Cat No. 16616-1-AP. After washing three times for 10 min each with wash buffer (450 nM NaCl, 20 mM phosphate buffer, and 0.3 % Triton X-100), slides were incubated with secondary antibody in GSDB for 60 min at room temperature in a wet and light-protected chamber. Slides were subsequently washed three times with the wash buffer and stained by diaminobenzidine, followed by counterstaining using hematoxylin to visualize nuclei.

## 2.6. Cell lines and cell culture

GBM tissues were obtained from excess surgical resection samples from patients at the Case Western Reserve University (Cleveland, OH) after review by neuropathology with appropriate consent and in accordance with an Institutional Review Board–approved protocol (090401). All patient studies were conducted in accordance with the Declaration of Helsinki. To minimize in vitro cell culture-based artifacts, patient-derived xenografts were propagated as a renewable source of GSCs. Short tandem repeat analyses were performed on the tumor model for authentication. Patient-derived primary GSCs, including MES28 and 387, were kindly provided by Dr. Jeremy N. Rich (UPMC) [30–35]. It is sufficient to support our research related to GSCs. These cell lines were cultured in Neurobasal medium (Gibco) supplemented with B27 without vitamin A (Gibco), EGF and bFGF (20 ng/mL each; R&D Systems), sodium pyruvate (Gibco, 11360070), and Glutamax (Gibco, 35050061) at 37 °C with 20 % oxygen and 5 % carbon dioxide. STR analyses were performed on each tumor model used in this article for authentication.

293FT cells (ThermoFisher Scientific, Cat# R70007, RRID: CVCL\_6911) were used to generate lentiviral particles as described in the method details section. 293FT cells were derived from embryonic kidney cells from a female human.

## 2.7. Radiation and TMZ treatments

Radiation and TMZ treatments were performed to evaluate the effects of dose and exposure time on the expression of the target gene. For radiation experiments, cells were either exposed to a fixed dose of 5 Gy and harvested at 0, 24, 48, 72, and 96 h to assess temporal responses, or harvested at a fixed time point of 24 h following varying doses of 0, 2, 5, 8, and 12 Gy to evaluate dose-dependent effects. For TMZ experiments, cells were treated with a fixed concentration of 0.4 mM and collected at 0, 12, 24, 36, and 48 h for temporal analysis, or exposed to varying concentrations of 0, 0.2, 0.4, 0.6, and 1 mM and harvested at 24 h for dose-response evaluation. All samples were processed in parallel for RNA extraction and RT-qPCR analysis, protein extraction and western blotting, as well as ELISA quantification, with at least three biological replicates per group.

## 2.8. Plasmids and lentiviral transduction

Lentiviral clones expressing either one of two nonoverlapping short hairpin RNAs (shRNAs) directed against human LGALS3 and human EGR1, or a nontargeting control shRNA (shCONT) that matches no expressed sequence in the human genome were obtained from Sigma-Aldrich. Nonoverlapping shRNAs were selected based on knockdown efficiency and were then used for all following experiments. The sequence of shRNAs used in this study were: shGal3-1 forward 5'-CCGGGCAGTACAATCATCGGGTTAACTCGAGTTAACCGATGATTG TACTGCTTTTGG-3' and reverse 3'-AATTCAAAAAGCAGTACAATCATC GGGTTAACTCGAGTTAACCGATGATTGTAAGTGC-5'; shGal3-2 forward 5'-CCGGGCAATACAAAGCTGGATAATACTCGAGTATTATCCAGCTTTG TATTGCTTTTGG-3' and reverse 3'-AATTCAAAAAGCAATACAAAG CTGGATAATACTCGAGTATTATCCAGCTTTGTAAGTGC-5'; shEGR1-1 forward 5'-CCGGCGACATCTGTGAAGAAAGTTCTCGAGAAGCTTTCTT CCACAGATGTCGTTTTTGG-3' and reverse 3'-AATTCAAAAACGACATC TGTGGAAGAAAGTTCTCGAGAAGCTTTCTCCACAGATGTCG-5'; shEGR1-2 forward 5'-CCGGCTGTCTACTATTAAGGCCTTTCTCGA GAAAGGCCTTAATAGTAGACAGTTTTTGG-3' and reverse 3'-AATT CAAAACTGTCTACTATTAAGGCCTTTCTCGAGAAAGGCCTTAATAG TAGACAG-5'. 293FT cells were used to generate lentiviral particles through co-transfection of the packaging vectors PAX2 and VSVG using a standard calcium phosphate transfection method in Neurobasal complete medium.

## 2.9. Quantitative RT-PCR

RNAiso Plus (Takara, 9109) was used to isolate total cellular RNA from cell pellets. The qScript cDNA Synthesis Kit (Quanta BioSciences) was used for reverse transcription into cDNA. Quantitative real-time PCR was performed using Applied Biosystems 7900HT cycler using SYBR-Green PCR Master Mix (Thermo Fisher Scientific). qPCR primers used in this study were: human LGALS3 forward 5'-GTGAAGCC-CAATGCAAACAGA-3' and reverse 5'-AGCGTGGGTAAAGTGAAGG-3'; human EGR1 forward 5'-GGTCAGTGGCCTAGTGAGC-3' and reverse 5'-GTGCCGCTGAGTAAATGGGA-3' and 18S RNA forward 5'-AACCCGTTGAACCCATT-3' and reverse 5'-CCATCCAATCGGTAG-TAGCG-3'.

## 2.10. Western blotting

Cells were lysed in RIPA buffer (50 mM Tris-HCl pH 7.5, 150 mM NaCl, 0.5 % NP-40, 50 mM NaF, protease inhibitors) on ice for 30 min. Lysates were centrifuged at 14,000×g (4 °C, 10 min), and supernatants collected. Protein concentration was determined using the Bradford assay (Bio-Rad). Equal amounts were mixed with Laemmli buffer, boiled, and resolved by SDS-PAGE (NuPAGE Bis-Tris Gels) before transfer to PVDF membranes. Membranes were blocked with 5 % milk in TBS-T (45 min), then incubated with primary antibodies (Galectin-3/LGALS3, CST #87985; EGR1, Proteintech #55117-1-AP;  $\beta$ -Tubulin, Abcepta #AM1031a) at 4 °C overnight. Blots were visualized using Bio-Rad Image Lab software and processed with Adobe Photoshop. Uncropped gels and blots images for Western Blots were shown in Supplementary File.

## 2.11. Enzyme-Linked immunosorbent Assay (ELISA)

Cells ( $2 \times 10^6$ /100 mm dish) were cultured for 24h. The supernatants were collected, and any floating cells were removed via 0.45- $\mu$ m filtration. The amount of Galectin-3 protein in the supernatant was determined using a Human Galectin-3 ELISA Kit (Absin, abs551016). All experiments were performed according to the manufacturer's instructions.

## 2.12. Isolation of human CD4<sup>+</sup> and CD8<sup>+</sup> T cells

Peripheral blood mononuclear cells (PBMCs) were isolated from heparinized whole blood of healthy donors via Ficoll-Paque PLUS density gradient centrifugation. CD4<sup>+</sup> and CD8<sup>+</sup> T cells were sequentially enriched through negative magnetic-activated cell sorting using the Human CD4<sup>+</sup> and CD8<sup>+</sup> T Cell Isolation Kits (STEMCELL Technologies, 17952 and 17953), following the manufacturer's protocol. Post-sort purity was validated by flow cytometry with >90 % target cell purity.

## 2.13. In vitro culture of CD4<sup>+</sup> and CD8<sup>+</sup> T cells

Purified CD4<sup>+</sup> and CD8<sup>+</sup> T cells were cultured in ImmunoCult-XF T Cell Expansion Medium (STEMCELL Technologies, 10981) supplemented with 10 ng/mL Human Recombinant IL-2 (STEMCELL Technologies, 78036), and  $1 \times$  Antibiotic-Antimycotic (Gibco, 15240062). Cells were stimulated with 25  $\mu$ L/mL ImmunoCult Human CD3/CD28 T Cell Activator (STEMCELL Technologies, 10971) and seeded at  $1 \times 10^6$  cells/mL in 12-well plates. Cultures were maintained at 37 °C with 20 % oxygen and 5 % carbon dioxide.

## 2.14. T cell-GSC co-culture system

Purified CD4<sup>+</sup> or CD8<sup>+</sup> T cells and GSCs were co-cultured in a transwell system (6-well, 3.0  $\mu$ m pore, Corning, 3414) using Neurobasal Medium. T cells (effector) were seeded in the upper chamber at specified effector-to-target (E:T) ratios, while GSCs (target) were plated in the

lower chamber. Cultures were maintained at 37 °C with 20 % oxygen and 5 % carbon dioxide for 24 h.

### 2.15. Flow cytometry analysis of T cell function

The T cell suspensions were stimulated with Leukocyte Activation Cocktail with BD GolgiPlug (BD Pharmingen, 550583) at 37 °C with 20 % oxygen and 5 % carbon dioxide for 4 h. Then cells were washed with BSA, stained for viability (Fixable Viability Stain 450, BD Horizon, 562247), followed by surface markers (BV510 Mouse Anti-Human CD3 [BD Horizon, 564713], BB515 Mouse Anti-Human CD45 [BD Horizon, 564585], BV650 Mouse Anti-Human CD4 [BD Horizon, 563875], APC-Cy<sup>TM</sup>7 Mouse Anti-Human CD8 [BD Pharmingen, 557834]) for 30 min, 4 °C. Intracellular staining (40 min, 4 °C dark) was performed after fixation/permeabilization: TNF- $\alpha$  (PE Mouse Anti-Human TNF, BD Pharmingen, 559321), IFN- $\gamma$  (PE- Cy<sup>TM</sup>7 Mouse Anti-Human IFN- $\gamma$ , BD Pharmingen, 557844), GZMB (APC anti-human/mouse Granzyme B Recombinant Antibody, Biolegend, 372204), and Ki67 (RB705 Mouse Anti-Ki-67, BD Horizon, 570280). Data were acquired on a BD FACSVerse flow cytometer and analyzed with FlowJo v10.8.1.

For *in vitro* experiments, functional marker expression was quantified as the proportion of double-positive cells, calculated by applying predefined thresholds to flow cytometry data and determining the percentage of events within intersecting gates. For *in vivo* experiments, expression levels were assessed by mean fluorescence intensity (MFI), extracted from fluorescence histograms of each gated T cell subset. Data from all biological replicates were included in statistical comparisons. Consistent gating strategies and threshold settings were applied across all samples to ensure reproducibility.

### 2.16. Flow cytometry analysis of GSC apoptosis

Following initial co-culture, T cells were isolated from the transwell system and re-co-cultured with untreated GSCs using identical conditions. Post-co-culture, GSCs from the lower chamber were collected and washed with cold PBS. Apoptosis was assessed using the Annexin V-FITC/PI Apoptosis Detection Kit (Yeason, 40302ES60) per manufacturer's protocol, then immediately analyzed on a BD FACSVerse flow cytometer. Viable (Annexin<sup>−</sup>/PI<sup>−</sup>), early apoptotic (Annexin V+/PI<sup>−</sup>), and late apoptotic/necrotic (Annexin V+/PI<sup>+</sup>) populations were quantified using FlowJo v10.8.1.

### 2.17. T Cell proliferation Assay

T cells were labeled with 5  $\mu$ M CFSE at  $1 \times 10^7$ /mL, incubated at 37 °C for 10 min (mixed every 5 min), and quenched with 10 % FBS-containing NBM. Cells were washed with PBS and NBM, followed by resuspension in IL-2-supplemented NBM. T cells were co-cultured with GSCs in Transwell plates for 72–96 h (medium replenished at 48 h). Post-culture, T cells were stained with anti-CD3/CD4/CD8 antibodies and analyzed via flow cytometry. Unstimulated CFSE-labeled T cells served as G0-phase proliferation controls.

### 2.18. RNA sequencing Analysis

Total RNA was extracted from GSCs preconditioned with 5 Gy irradiation and 72-h culture using RNAiso Plus (Takara, 9109). RNA quality and library integrity were validated via Agilent 4200 Bioanalyzer prior to sequencing on an Illumina NovaSeq 6000 (150 bp paired-end). Raw reads were filtered, aligned to GRCh38 (HISAT2 v2.0.4), and quantified (StringTie v1.3.3b) with TMM normalization. Differentially expressed genes were identified using DESeq2 (Log2FC > 1, adjusted P < .05).

### 2.19. Chromatin immunoprecipitation quantitative real-time PCR (ChIP-qPCR)

ChIP was performed using a SimpleChIP Enzymatic Chromatin IP Kit (Magnetic Beads) (Cell Signaling Technology, 9003S) with antibodies against EGFR1. Goat IgG was used as isotype control. Promoter fragments for LGALS3(Gal3) were amplified by qRT-PCR. Data were expressed as fold enrichment relative to IgG control.

### 2.20. Animal models

Intracranial xenografts were established in 4-6-week-old female NCG (NOD/ShiLtJGpt-Prkdc<sup>em26Cd52</sup>Il2rg<sup>em26Cd22</sup>/Gpt, Strain NO. T001475, GemPharmatech, Nanjing, China) mice under an animal protocol approved by the Institutional Animal Care and Use Committee (IACUC-2006033-2) at Nanjing Medical University in accordance with NIH and institutional guidelines.

On day 0, a cranial guide screw was surgically implanted into the right cerebral cortex, followed by intracranial injection of  $5 \times 10^4$  preconditioned human GSCs suspended in 10  $\mu$ l PBS at a depth of 3.5 mm. Tumor formation was confirmed by bioluminescence imaging on day 1. On day 3 post-implantation, tumor-bearing mice received radiotherapy at 2 Gy per session every 3 days, with a total cumulative dose of 12 Gy. Concurrently, starting from day 7 after tumor implantation,  $8 \times 10^5$  purified human T cells ( $3.2 \times 10^5$  CD4<sup>+</sup> and  $4.8 \times 10^5$  CD8<sup>+</sup>) were injected intracranially into the tumor site via the pre-implanted guide screw, with weekly booster injections administered using the same parameters.

Mice were maintained under specific pathogen-free (SPF) barrier conditions by animal husbandry staff at the Nanjing Medical University, with strictly controlled environmental parameters: temperature 20–26 °C, humidity 30–70 %, and a 12-h light/dark cycle, and housed at a density of no more than five animals per cage. Animals were monitored until neurological signs were observed in any one of the groups, at which point two mice of each group were selected randomly and their brains were harvested and fixed in 4 % formaldehyde, cryopreserved in 30 % sucrose, and then cryosectioned. Hematoxylin and eosin (H&E) staining was performed on sections for histological analysis. In parallel survival experiments, mice were observed until the development of neurological signs.

### 2.21. Drug treatment

ML264 (MedChemExpress, HY-19994) was administered intraperitoneally at 5 mg/kg every 2 days starting from day 9 post-implantation, continuing until mice exhibited neurological symptoms.

Relatlimab (MedChemExpress, HY-P99156) was delivered intracranially at 3  $\mu$ g/3  $\mu$ l every 3 days via the guide screw starting from day 10 post-implantation, also continuing until neurological symptoms appeared.

### 2.22. Cell suspension preparation from mice tissue

Fresh brain specimens were mechanically dissociated into 1–2 mm<sup>3</sup> fragments and enzymatically digested at 37 °C for 30 min using a cocktail containing collagenase IV (1 mg/mL, Gibco, 17104019), DNase I (20 U/mL, Sigma-Aldrich, DN25), and hyaluronidase (0.01 %, Solarbio, H8160) in DMEM basal medium. Post-digestion, cell suspensions were sequentially filtered through a 70- $\mu$ m cell strainer (Falcon, 352350) and treated with Myelin Removal Beads (Miltenyi Biotec, 130-109-398) following manufacturer's protocol for myelin debris elimination. Erythrocyte contamination was removed using ACK lysing buffer (Beyotime, C3702). Purified cells were resuspended in FACS buffer (PBS supplemented with 2 % FBS) for downstream applications.

### 2.23. Quantification and statistical analysis

Power calculations based upon previous *in vivo* studies in our models were utilized to predetermine sample sizes. The studies were designed with 80 % power to detect a difference of 20 % given a 10 % standard deviation at a significance level of  $\alpha = 0.05$ . Kaplan-Meier survival curves were generated using Prism software and a log-rank test was performed to assess statistical significance between groups. For other studies, a two-sided unpaired Student's *t*-test was used to assess differences between groups. Data distribution was assessed for normality using the Shapiro-Wilk test. Precise experimental details (number of animals or cells and experimental replication) are provided in the figure legends or in the Methods sections above. P values are detailed in the figure legends. P values < 0.05 were considered to be significant.

## 3. Results

### 3.1. Suppressive immune checkpoint LAG3 is a key factor driving T cell exhaustion in recurrent GBM

To characterize and compare the T cell status in newly diagnosed GBMs and recurrent GBMs, we analyzed two scRNA-seq datasets of GBM: GSE182109 (22 samples from 11 newly diagnosed and 15 samples from 4 recurrent GBM patients) and GSE163120 (12 newly diagnosed and 5 recurrent GBM samples) (Fig. 1A–B). Patient-derived GBM specimens contained diverse immune cell clusters, predominantly consist of TAMs and T cells. Considering the significant tumor-killing role of T cells, we further analyzed the distribution of GBM-infiltrating T cells in newly diagnosed and recurrent tumors (Fig. 1C–D). Comparing the exhaustion scores of newly diagnosed and recurrent GBM-infiltrating T cells, we found that T cells from recurrent GBM exhibited a more exhausted status than those from primary GBM (Fig. 1E–H).

To identify key drivers of T cell exhaustion in recurrent GBM, we performed an integrative multiomics analysis of GBM-infiltrating T cells from both newly diagnosed and recurrent states across GSE182109 and GSE163120 ( $p_{\text{val\_adj}} < 0.05$ ;  $\log_2\text{FC} > 0.25$ ) and the inhibitory immune checkpoint list. We identified LAG3 as the key factor driving T cell exhaustion in recurrent GBM (Fig. 1I). Furthermore, UMAP plots and scatterplots showed that LAG3 expression was upregulated in T cells from recurrent GBM (Fig. 1J–M). Based on the traditional typing of T cells [36], we characterized LAG3 expression in  $\text{CD4}^+$  and  $\text{CD8}^+$  T cells from newly diagnosed and recurrent GBMs. It showed that both  $\text{CD4}^+$  and  $\text{CD8}^+$  T cells had elevated LAG3 expression in the relapsed samples (Supplementary Fig. 1F–I, Fig. 1N–Q). Consistent with these results, LAG3 expression was significantly enriched in Tex-high versus Tex-low T cell subpopulations in both GSE182109 and GSE163120 (Fig. 1R). Moreover, Pearson correlation analysis in IDH-wildtype GBM samples from the TCGA cohort revealed a positive association between Tex score and LAG3 expression (Fig. 1S). Furthermore, using immunohistochemical staining of tissue microarrays from 18 paired patients with primary and recurrent GBM specimens, we identified that LAG3 expression was significantly higher in recurrent tissues than in primary tissues (Fig. 1T–U). Taken together, these data demonstrate that inhibitory immune checkpoint LAG3 is a key driver of both  $\text{CD4}^+$  and  $\text{CD8}^+$  T cell exhaustion in recurrent GBM.

Gal3, the LAG3 ligand, is specifically upregulated in recurrent GBM by radiation.

Given that there are five recognized ligands for LAG3, we sought to identify which ligand's expression changed in GBM recurrence [37]. Analysis of the GSE182109 revealed that only Gal3 was elevated in recurrent GBM samples, while expressions of FGL1, CLEC4G, SNCA or MHC-II remained unchanged (Supplementary Fig. 2A–D and Fig. 2A–C). Furthermore, validation using the CGGA database of primary and recurrent samples, along with RNA-seq data of GSC lines with radiation treatment also showed upregulation of Gal3 (Supplementary Fig. 2E–F).

Since recurrent GBM is commonly accompanied by effective

intervention with radiotherapy and TMZ chemotherapy, we further explored which treatment modality contributed to elevated Gal3 expression in GBM. GSEA indicated a positive correlation between Gal3 expression and response to radiotherapy (Fig. 2D). Consistently, given the vital role of GSCs in GBM recurrence, we treated two GSC lines (MES28 and 387) with irradiation at varying doses and time points. It demonstrated that Gal3 expression was enhanced in GSCs following radiation treatment, at both mRNA and protein levels, in a dose- and time-dependent manner (Fig. 2E–J). In contrast, we also found that TMZ treatment of the same GSC lines at different dosage and durations, did not increase Gal3 expression at the mRNA, protein or secretory level (Supplementary Fig. 3A–F). Collectively, these results suggest that among the five LAG3 ligands, Gal3 is specifically upregulated in recurrent GBM and in irradiated GSCs.

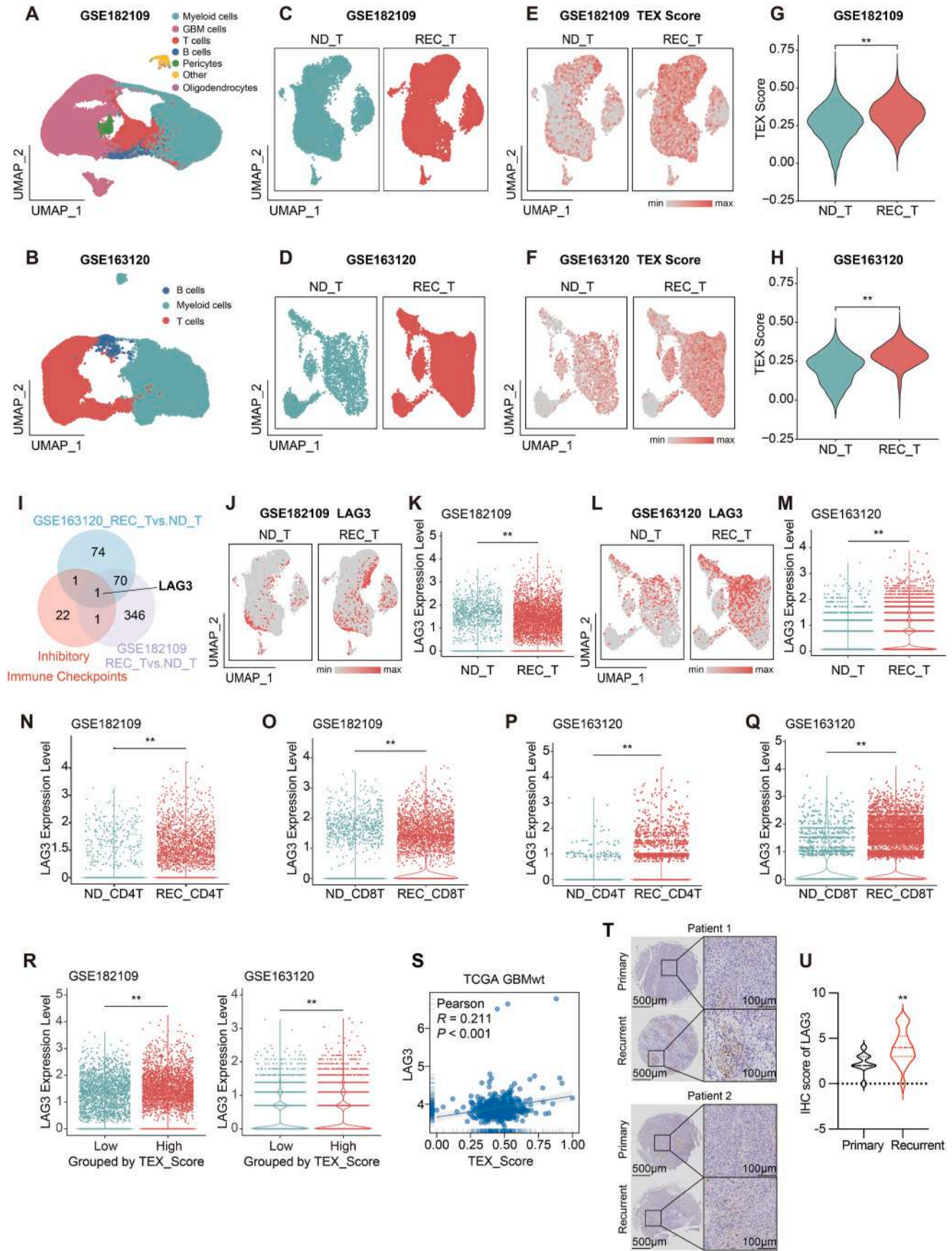
### 3.2. Gal3 in GSCs inhibits cytotoxic capacity of $\text{CD4}^+$ / $\text{CD8}^+$ T cells

To investigate the potential functions of Gal3, we performed loss-of-function and overexpression experiments. As expected, silencing Gal3 using two non-overlapping shRNAs reduced the mRNA and protein levels in two GSC lines (MES28 and 387) (Supplementary Fig. 4A–B). To determine the appropriate concentration for recombinant Gal3 supplementation, we quantified Gal3 secretion before and after Gal3 knock-down following radiation treatment (Supplementary Fig. 4C). In light of the correlation between the immune checkpoint LAG3 and T-cell activity, we used primary  $\text{CD4}^+$  and  $\text{CD8}^+$  T cells sorted from PBMCs from healthy donors (Supplementary Fig. 4D–E) to co-culture with GSCs, followed by flow cytometry-based functional assays based on T-cell function to assess T-cell-mediated cytotoxicity.

First, we characterized the changes in the expression of T cell-associated effectors (TNF- $\alpha$ , IFN- $\gamma$ , Granzyme B) and a proliferation marker (Ki-67) in PBMC-derived  $\text{CD4}^+$  or  $\text{CD8}^+$  T cells after co-culture with irradiated GSCs. Gal3 knockdown in irradiated MES28 and 387 cells enhanced the expression of TNF- $\alpha$ , IFN- $\gamma$ , Granzyme B, and Ki-67 in co-cultured  $\text{CD4}^+$  and  $\text{CD8}^+$  T cells (Supplementary Fig. 6A–D); while recombinant Gal3 protein (rGal3) treatment in GSCs suppressed the expression of the T cell-associated effectors above (Fig. 3A–D), indicating that Gal3 inhibition increases cytokine production and proliferation in T cells. To directly test cytotoxic function, we re-isolated T cells after co-culture with irradiated, Gal3-knockdown GSCs and then re-cultured them with untreated GSCs. The results indicated that  $\text{CD4}^+$  and  $\text{CD8}^+$  T cells co-cultured with irradiated, Gal3-knockdown GSC induced more apoptosis in GSCs, indicating stronger tumor killing ability (Supplementary Fig. 6E). This effect was overcome by rGal treatment (Fig. 3E). Using a CFSE assay after co-culture of T cells with treated GSC cells, we revealed that Gal3 knockdown in GSCs promoted the proliferation of  $\text{CD4}^+$  and  $\text{CD8}^+$  T cells (Supplementary Fig. 6F). Collectively, these data support that GSC-derived Gal3 inhibits cytotoxic capacity of both  $\text{CD4}^+$  and  $\text{CD8}^+$  T cells.

### 3.3. Gal3 in GSCs reduces cytotoxic capacity of $\text{CD4}^+$ / $\text{CD8}^+$ T cells in vivo

Based on the *in vitro* co-culture results, we next validated the functional role of Gal3 in an *in vivo* xenograft model. Irradiated, Gal3-knockdown GSCs were co-implanted with or without T cells into the brains of immunocompromised mice (NCG mice) (Fig. 4A). Mice implanted with Gal3-knockdown GSCs and T cells exhibited prolonged survival and reduced tumor progression (Fig. 4B–D). These data indicated that Gal3 plays a vital role in helping irradiated GSCs inhibit the efficiency of T cell in xenograft models. After isolating tumor-infiltrating  $\text{CD4}^+$  and  $\text{CD8}^+$  T cells from mouse tumor, we analyzed the expression of markers associated with T cell activation and cytokine production. The expression of TNF- $\alpha$ , IFN- $\gamma$ , granzyme B, and Ki-67 were upregulated in T cells isolated from mice implanted with Gal3-knockdown GSCs and T cells compared to the T cells isolated from mice in control group.



(caption on next page)

**Fig. 1.** LAG3 is a key factor driving T cell exhaustion in recurrent GBM.

A-B, UMAP projections of immune cell clusters in fresh GBM specimens. (A) 11 newly diagnosed cases ( $n = 22$  specimens) and 4 recurrent cases ( $n = 15$  specimens) from GSE182109. (B) 12 newly diagnosed and 5 recurrent GBM samples from GSE163120. C-D, UMAP visualization of GBM-infiltrating T cells in newly diagnosed and recurrent states. Data were derived from GSE182109 (C) and GSE163120 (D). E-F, UMAP visualization of the TEX score of GBM-infiltrating T cells in newly diagnosed and recurrent states. Data were derived from GSE182109 (E) and GSE163120 (F). G-H, Violin plot illustrated exhaustion scores of newly diagnosed and recurrent GBM-infiltrating T cells. Data were derived from GSE182109 (G) and GSE163120 (H).  $**P < .01$ . I, Venn diagram showed the overlap of GSE182109 GBM-infiltrating T cells in newly diagnosed and recurrent states ( $p_{\text{val adj}} < 0.05$ ;  $\log_2\text{FC} > 0.25$ ), GSE163120 GBM-infiltrating T cells in newly diagnosed and recurrent states ( $p_{\text{val adj}} < 0.05$ ;  $\log_2\text{FC} > 0.25$ ) and the inhibitory immune checkpoint list. J-M, LAG3 expression patterns. (J-K) UMAP projections and scatter plots of LAG3 expression in GBM-infiltrating T cells from GSE182109. (L-M) Corresponding visualizations for GSE163120.  $**P < .01$  for state comparisons. N-O, Scatterplot illustrated the expression of LAG3 in GBM-infiltrating  $\text{CD4}^+$  T cells (N) and  $\text{CD8}^+$  T cells (O) in newly diagnosed and recurrent states. Data were derived from GSE182109.  $**P < .01$ . P-Q, Scatterplot illustrated the expression of LAG3 in GBM-infiltrating  $\text{CD4}^+$  T cells (P) and  $\text{CD8}^+$  T cells (Q) in newly diagnosed and recurrent states. Data were derived from GSE163120.  $**P < .01$ . R, Scatterplot illustrated that LAG3 expression was significantly higher in Tex-high than Tex-low T cell subpopulations in GSE182109 and GSE163120.  $**P < .01$ . S, Scatterplot illustrated the result of Pearson correlation analysis between Tex score and LAG3 expression in IDH-wildtype GBM samples from the TCGA dataset. T, Representative images of immunohistochemical staining of LAG3 in paired primary and recurrent GBM patients. U, Statistical chart illustrated the IHC Score of LAG3 in paired primary and recurrent GBM patients ( $n = 18$  paired).  $**P < .01$ .

This result further supports that GSC-derived Gal3 reduces cytotoxic capacity of  $\text{CD4}^+$  and  $\text{CD8}^+$  T cells *in vivo* (Fig. 4E-F, Supplementary Fig. 8).

### 3.4. EGR1 transcriptionally upregulated Gal3 expression in irradiated GSCs

To explore the mechanism of elevated Gal3 expression in GBM after radiotherapy, we integrated multi-omics analysis from three datasets: differentially expressed genes from RNA-seq of irradiated vs. control GSCs (MES28, 387;  $p_{\text{val adj}} < 0.05$ ;  $\log_2\text{FC} > 1$ ), the CGGA GBM mRNA expression dataset ( $p < .05$ ;  $R > 0.2$ ) and gene sets correlated with radiation response (Fig. 5A). We performed the correlation analysis in the CGGA database and RNA-seq data (GSE294744), which revealed a higher correlation between EGR1 and Gal3 ( $p < .05$ ;  $R = 0.515$ ) between FOS and Gal3 ( $p = .022$ ;  $R = 0.234$ ) (Fig. 5B-C, Supplementary Fig. 9E-F). We identified that EGR1 and FOS as the potential key factors regulating elevated Gal3 expression in GSCs after radiation treatment. We further use the JASPAR database to computationally predict the binding potential of EGR1 and FOS to the Gal3 promoter [38]. As shown in Fig. 5D, the prediction scores for EGR1 were higher than those for FOS. Taken together, we hypothesized that the elevated expression of EGR1 is the main factor resulting in upregulation of Gal3 in irradiated GSCs.

To verify the hypothesis, we first examined EGR1 expression in irradiated GSCs. The results revealed that both mRNA and protein level of EGR1 were increased in GSCs following radiation treatment, consistent with the RNA-seq data (Fig. 5E-F). To confirm the direct binding of EGR1 to the Gal3 promoter, we performed chromatin immunoprecipitation assays in GSCs followed by PCR for Gal3, revealing enrichment of EGR1 at the Gal3 promoter (Fig. 5G). We next considered whether EGR1 could directly regulate Gal3 expression in GSCs. Knockdown of EGR1 using two non-overlapping shRNA significantly reduced both mRNA and protein levels of Gal3 in GSCs (Fig. 5H-I). Furthermore, we explored whether pharmacologic inhibition of EGR1 by its specific antagonist, ML264 [39], could impact the expression of Gal3 in GSCs. The results showed that treatment with ML264 downregulated both EGR1 and Gal3 at both mRNA and protein level in GSCs (Fig. 5J-L).

Inhibition of EGR1 in irradiated GSCs synergizes with LAG3 blockade to improve the prognosis of GBM bearing mice.

Given that GSCs secreted Gal3 causing the exhaustion of  $\text{CD4}^+$  and  $\text{CD8}^+$  T cells, we further hypothesized EGR1 expression in GSCs would also affect the function of  $\text{CD4}^+$  and  $\text{CD8}^+$  T cells. We isolated primary  $\text{CD4}^+$  and  $\text{CD8}^+$  T cells from PBMCs of healthy donors for co-culture with GSCs. Flow cytometry analysis was performed to evaluate T cell cytotoxicity against GSCs. EGR1 knockdown in irradiated GSCs

enhanced the expression of  $\text{TNF-}\alpha$ ,  $\text{IFN-}\gamma$ , Granzyme B, and Ki-67 in co-cultured T cells (Supplementary Fig. 10A-D), indicating augmented cytokine production in both  $\text{CD4}^+$  and  $\text{CD8}^+$  T cells. To assess cytotoxic efficacy, T cells that had been co-cultured with irradiated, EGR1-KD GSCs were isolated and re-cultured with untreated GSCs. These effector T cells revealed significantly increased apoptosis induction against GSCs compared to controls (Supplementary Fig. 10E), demonstrating enhanced anti-tumor activity. In summary, EGR1 expression in GSCs also inhibits cytotoxic capacity of  $\text{CD4}^+$  and  $\text{CD8}^+$  T cells.

Based on the findings described above, we speculated that ML264 combined with anti-LAG3 antibody could enhance the efficacy of radiotherapy in this NCG mouse model (Fig. 6A). We selected ML264 for preclinical study due to its ability to penetrate the blood-brain barrier [40]. Relatlimab is a well-recognized ICB monoclonal antibody that blocks LAG3 [41]. Mice implanted with irradiated GSCs and T cells were treated with ML264, with or without relatlimab. As expected, the combination treatment resulted in a significantly longer survival than the monotherapy (Fig. 6B). Bioluminescence imaging demonstrated a slowdown in tumor growth in the ML264 and relatlimab groups at 25 and 50 days, and a significant reduction in tumor volume in the combination group, correlating with prolonged overall survival (Fig. 6C-D).

To determine the potential clinical relevance of Gal3, we interrogated the relationship between Gal3 expression and patient prognosis. Gal3 expression positively correlated with tumor grade in the CGGA, TCGA GBM LGG (low-grade glioma), Rembrandt and Gravendeel databases (Fig. 6E-H). High expression of Gal3 was associated with poor prognosis in tumor patients in multiple databases including CGGA, TCGA, Rembrandt, and Gravendeel GBM data sets (Fig. 6I-L). Taken together, Gal3 is a promising therapeutic target, which may inform the development of therapeutic strategies for GBM.

## 4. Discussion

GSCs represent a paramount therapeutic challenge in GBM management, characterized by their marked cellular heterogeneity, intrinsic resistance to conventional chemo- and radiotherapy, and potent tumor-repopulating capacity [42-44]. Despite several reports suggesting that immunotherapies targeting ICBs may influence GSC biology [45-48], ICB-based monotherapy or combination therapy rarely show satisfactory results in clinical trials for GBM patients, and relapse rates remain high [22,49-51]. This suggests that the mechanism of GSC resistance to ICB remains unclear. Here, we performed scRNA-seq analysis and revealed a significantly elevated exhaustion phenotype in T cells from recurrent GBM, which correlated with LAG3 upregulation. Mechanistically, EGR1-driven Gal3 overexpression in irradiated GSCs emerged as a critical mediator for T-cell dysfunction. These findings provide a

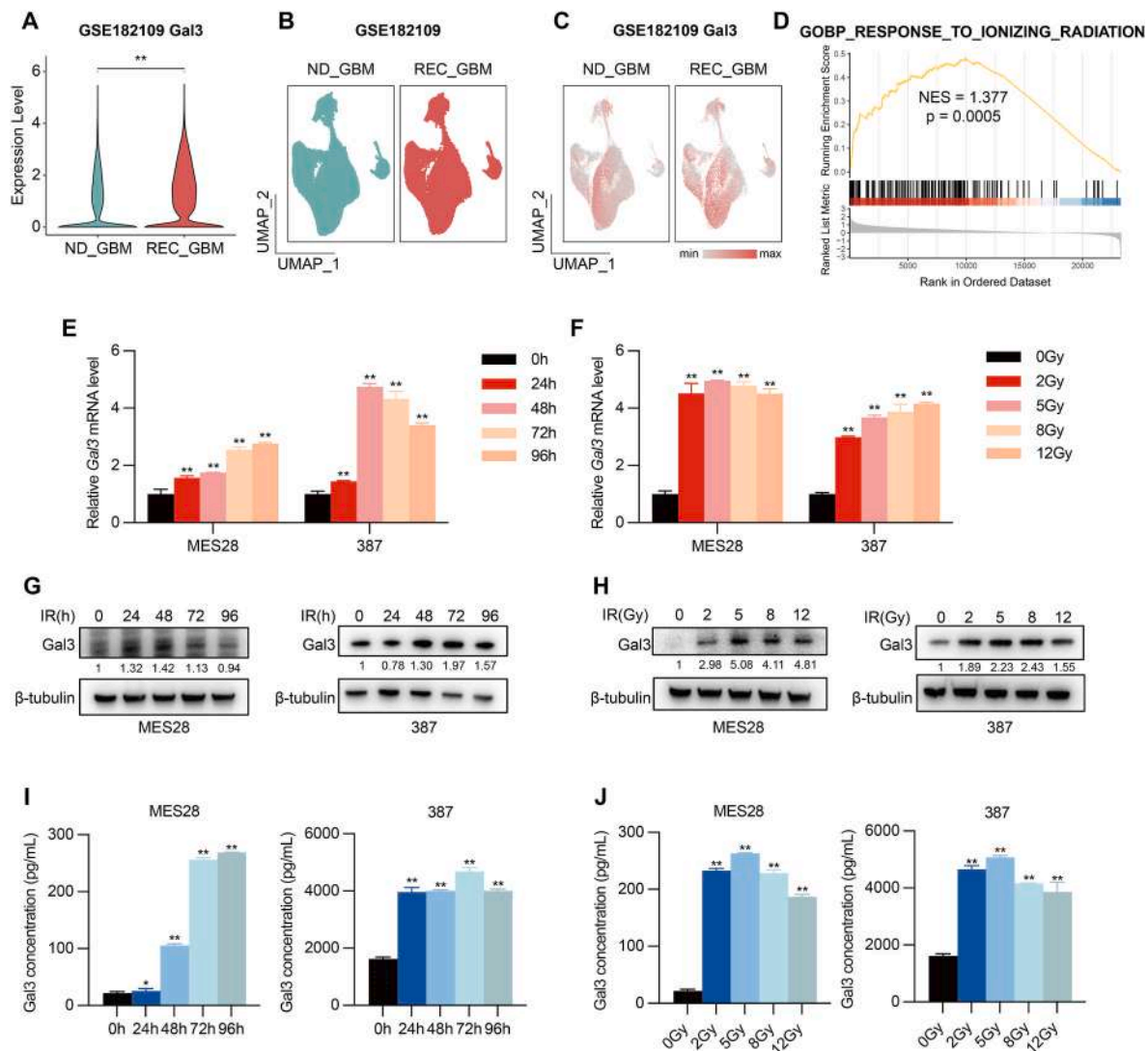


**Fig. 2.** Gal3 is upregulated by radiation in GSCs.

A, Violin plot illustrated the expression of Gal3 in newly diagnosed GBM cells and recurrent GBM cells. \*\* $P < .01$ .

B, UMAP visualization of GBM cells in newly diagnosed and recurrent states.

C, UMAP visualization of Gal3 expression across GBM cells in newly diagnosed and recurrent states.

D, GSEA showed the correlation between the expression of Gal3 and the response to radiotherapy.

E, RT-qPCR quantification of Gal3 mRNA levels after different times of radiation treatment in GSCs. \*\* $P < .01$ .

F, RT-qPCR quantification of Gal3 mRNA levels after different doses of radiation treatment in GSCs. \*\* $P < .01$ .

G, Protein levels of Gal3 were assessed by immunoblotting after different times of radiation treatment in GSCs.

H, Protein levels of Gal3 were assessed by immunoblotting after different doses of radiation treatment in GSCs.

I, ELISA analysis of Gal3 after different times of radiation treatment in GSCs. \* $P < .05$ , \*\* $P < .01$ .

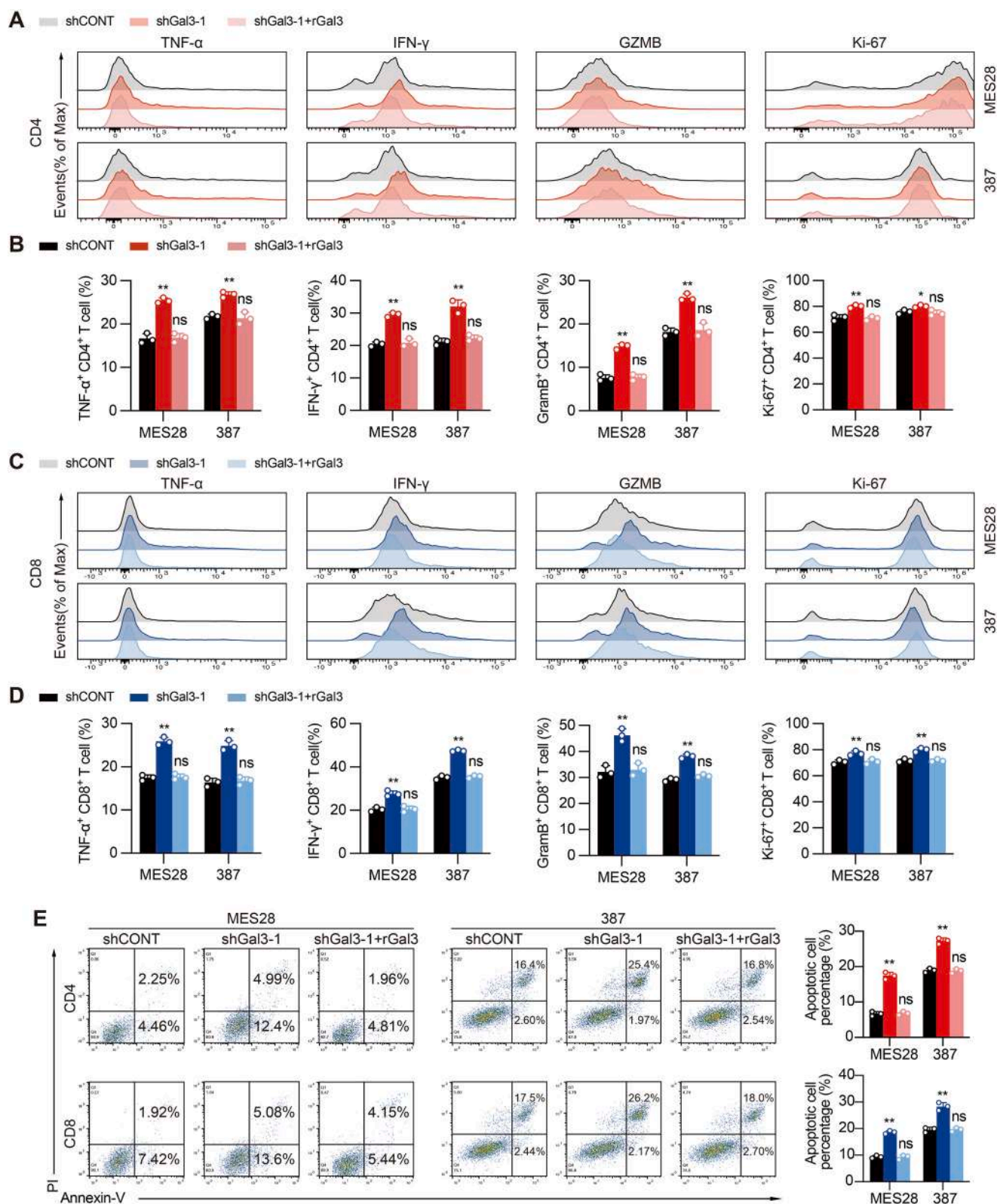
J, ELISA analysis of Gal3 after different doses of radiation treatment in GSCs. \*\* $P < .01$ .

mechanistic rationale for targeting the Gal3–LAG3 axis and its upstream regulator to reverse T-cell exhaustion and improve GBM prognosis.

LAG3 (also known as CD223) is expressed on multiple immune cells, including CD4<sup>+</sup> and CD8<sup>+</sup> T cells, exerting various biological influences on T cell functionality. LAG3 typically exerts inhibitory effects and contributes to T cell exhaustion [52,53]. As a co-inhibitory receptor implicated in T-cell exhaustion, LAG3 has been extensively documented in prior studies to correlate with inferior overall survival across solid malignancies [54,55]. However, its prognostic value demonstrates marked heterogeneity across different cancer types [56]. As a result, monoclonal antibodies targeting LAG3 are diverse and have demonstrated clinical efficacy in the treatment of specific cancers [51,57–59]. Our study shows that LAG3 functions as a pivotal determinant of T-cell exhaustion in recurrent GBM. Preclinical validation using the anti-LAG3 monoclonal antibody relatlimab *in vivo* confirmed its

immunomodulatory activity and antitumor efficacy. These findings not only identify the central role of GSCs in the radiation-induced micro-environment remodeling but also provide novel mechanistic insights into immune microenvironment dysregulation following tumor recurrence.

Gal3, a prototypic member of the galectin family, functions as a secreted  $\beta$ -galactoside-binding lectin that modulates cellular homeostasis by regulating cell cycle dynamics and apoptosis resistance. The oncogenic potential of Gal3, particularly its ability to stimulate tumor cell proliferation, epithelial-mesenchymal transition, and metastatic dissemination, has established it as a critical determinant in cancer progression [60,61]. Furthermore, extracellular Gal3 functions as a pivotal orchestrator of tumor-induced immunosuppressive programming, critically contributing to malignant immune evasion. In this study, tumor-derived Gal3 interacts with LAG3 on effector T cells to suppress



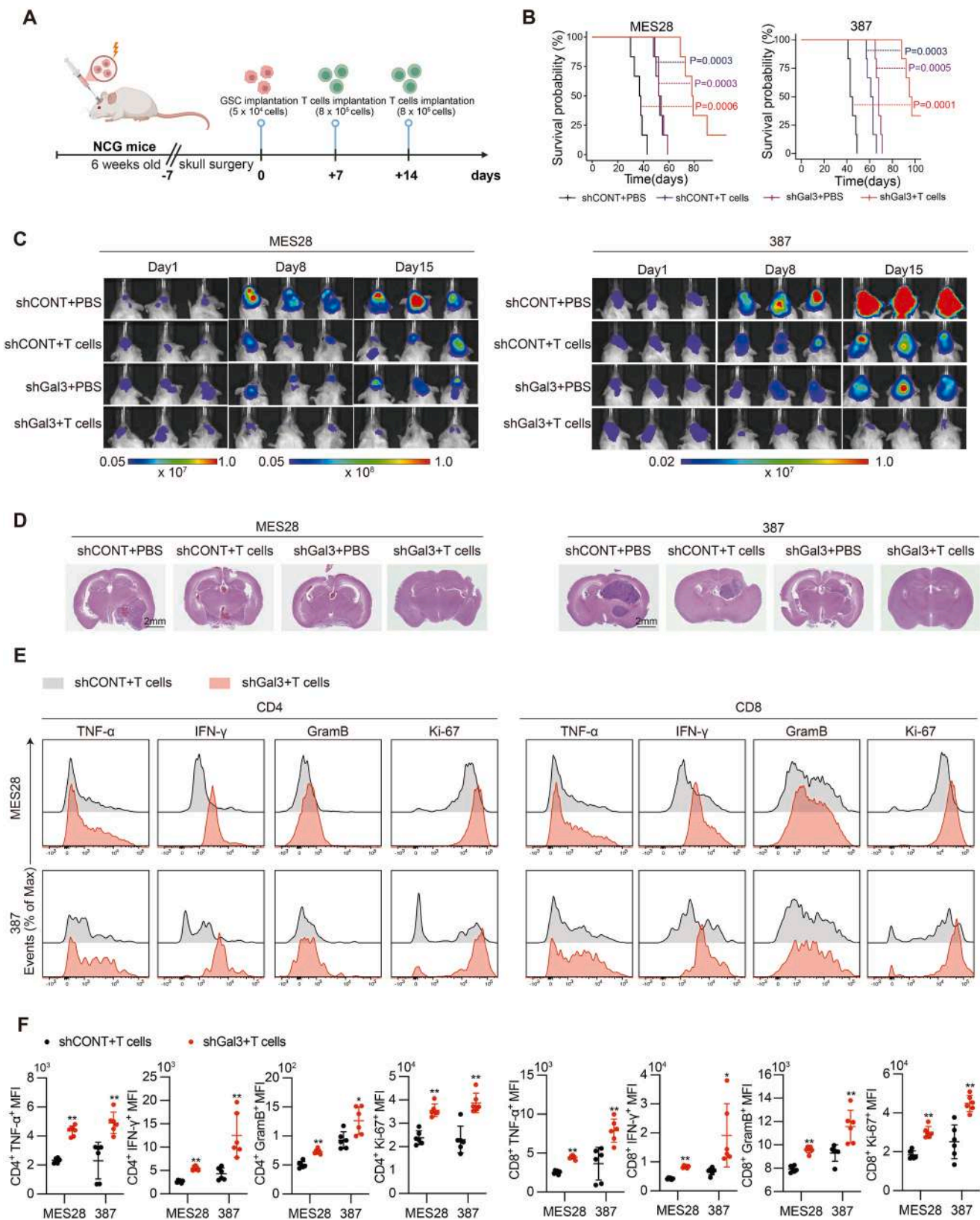


**Fig. 4.** Gal3 in GSCs reduces cytotoxic capacity of  $CD4^+/CD8^+$  T cells *in vivo*. A, Illustration of the in situ GBM model in immunocompromised mice and treatment with T cells. B, Kaplan–Meier survival curves of immunodeficiency mice with intracranial MES28 or 387 irradiated GSCs expressing shCONT + PBS, shCONT + T cells, shGal3+PBS and shGal3+T cells ( $n = 6$  per group). C, In vivo bioluminescent imaging of tumor growth was performed in NCG mice bearing G xenografts derived from MES28 or 387 irradiated GSCs transduced with shCONT or shGal3, with or without T cell co-implantation, on days 1, 8, and 15 ( $n = 6$  per group). D, Representative images of H&E staining of mouse brains collected on day 25 after transplantation of MES28 or 387 irradiated GSCs transduced with shCONT or shGal3, with or without T cell co-implantation. Scale bar, 2 mm. ( $n = 6$  per group). E–F, Representative histogram (E) and quantification (F) of the expression of the indicated molecules in  $CD4^+$  or  $CD8^+$  T cells isolated from the abovementioned GBM model ( $n = 6$  per group). \* $P < .05$ , \*\* $P < .01$ .

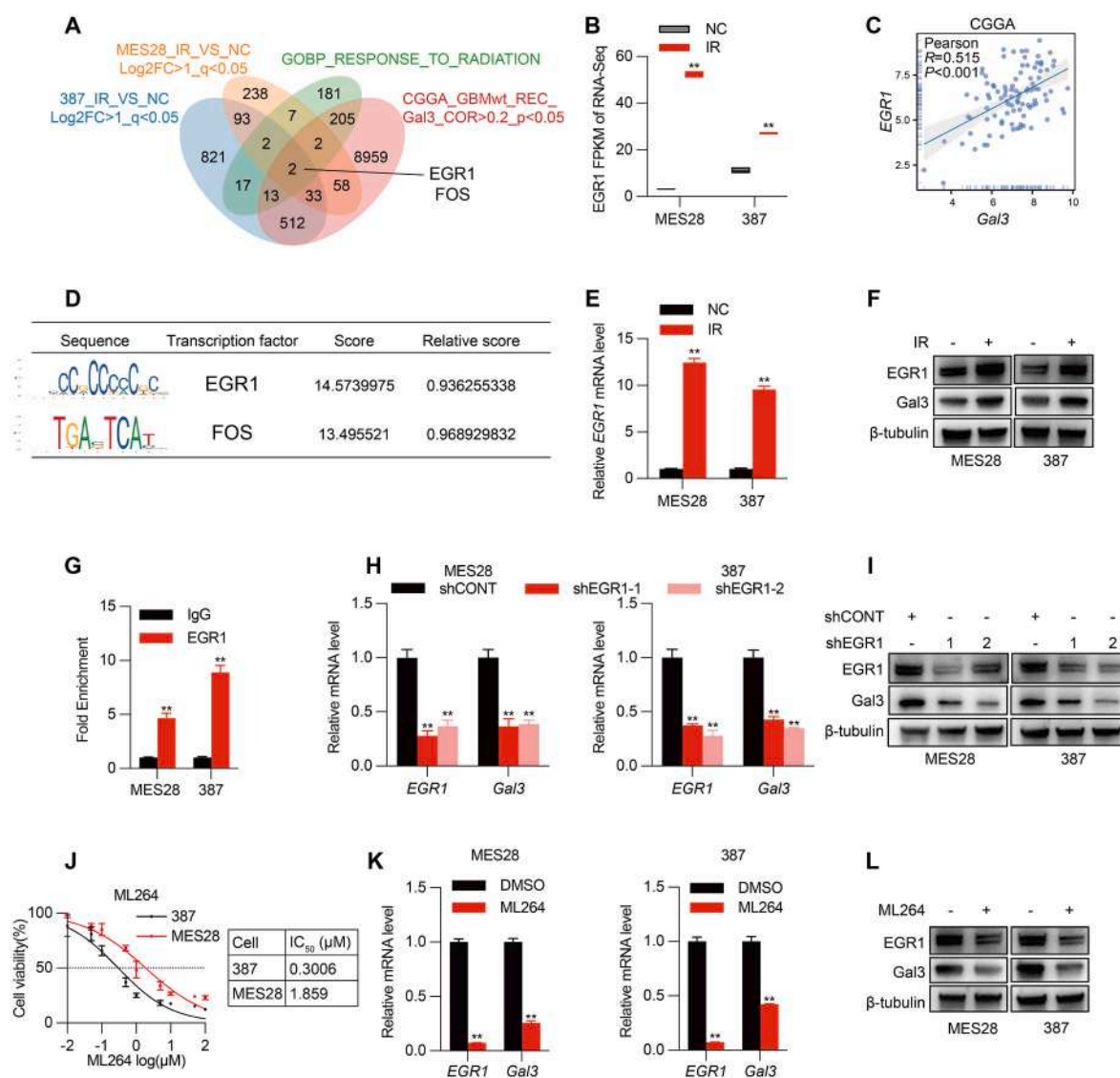
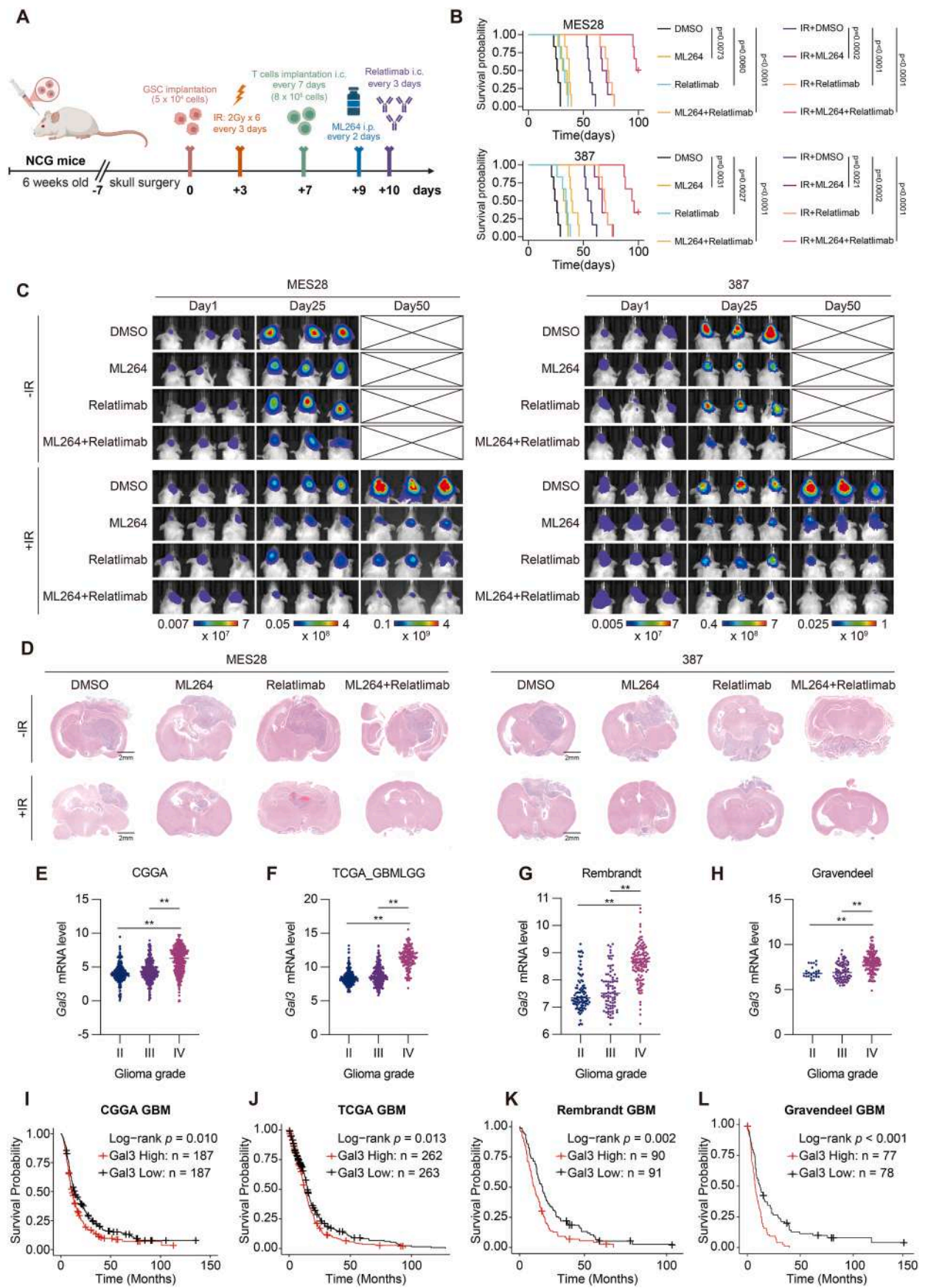


**Fig. 5.** Elevated Gal3 expression in irradiated GSCs is associated with elevated expression of the EGR1. **A**, Venn diagram showed the overlap of RNA sequencing data from differential genes in MES28 GSCs before and after radiation treatment ( $p_{\text{val,adj}} < 0.05$ ;  $\log_2\text{FC} > 1$ ), RNA sequencing data from differential genes in 387 GSCs before and after radiation treatment ( $p_{\text{val,adj}} < 0.05$ ;  $\log_2\text{FC} > 1$ ), CGGA GBM mRNA expression data set ( $p < .05$ ;  $R > 0.2$ ) and genes correlated with response to radiation. **B**, RNA-Seq data showed the expression of EGR1 before and after radiotherapy in MES28 and 387 GSCs. Data were derived from GSE294744.  $**P < .01$ . **C**, Correlation between the expression of EGR1 and Gal3. Analysis of gene expression in CGGA datasets. **D**, Predicted binding motif of Gal3 promoter. **E**, RT-qPCR quantification of *EGR1* mRNA levels before and after radiation treatment in MES28 and 387 GSCs.  $**P < .01$ . **F**, Protein levels of EGR1 were assessed by immunoblotting before and after radiation treatment in MES28 and 387 GSCs. **G**, EGR1 binds directly to promoter regions of Gal3. Cross-linked chromatin was prepared from MES28 and 387 GSCs, and then immunoprecipitated using an *anti*-EGR1 antibody or goat IgG control followed by real-time PCR using primers specific to promoter regions of Gal3. Data are presented as mean  $\pm$  SEM from 3 independent experiments.  $**P < .01$ . **H**, RT-qPCR quantification of mRNA levels of *EGR1* and *Gal3* in MES28 and 387 GSCs with EGR1 knockdown.  $**P < .01$ . **I**, Immunoblot showing knockdown of EGR1 in MES28 and 387 GSCs decreased the protein levels of Gal3. Tubulin was used as a loading control. **J**, IC<sub>50</sub> determination of ML264 in GSCs. **K**, RT-qPCR quantification of mRNA levels of *EGR1* and *Gal3* in MES28 and 387 GSCs treated with ML264.  $**P < .01$ . **L**, Immunoblot showing treated with ML264 in MES28 and 387 GSCs decreased the protein levels of Gal3 and EGR1. Tubulin was used as a loading control.

their cytotoxic capacity and proliferative potential, thereby attenuating anti-tumor immunity. Moreover, tumor-derived Gal3 has been demonstrated to orchestrate immune privilege by reprogramming macrophage polarization toward an immunosuppressive M2-like phenotype, thereby constituting a pivotal immunosuppressive mechanism in tumor micro-environment remodeling [62–64]. Our study dissects the dynamic evolution of T cell exhaustion in recurrent GBM, with a focus on Gal3-mediated modulation of T lymphocyte functionality. While corroborating prior observations that tumor-associated Gal3 suppresses T cell responses [65–67], we provide novel mechanistic insights into the Gal3-LAG3 regulatory circuitry within the GBM ecosystem. Specifically, we demonstrate that radiation-induced upregulation of EGR1

potentiates Gal3 expression in recurrent GBM, and that Gal3, through engagement with LAG3 enforces a profoundly exhausted phenotype in T cells, thereby undermining the therapeutic efficacy of ICB. Building upon the established efficacy of EGR1 inhibitor ML264 in colorectal cancer management [39,68,69], our study introduces an innovative combinatorial therapeutic approach by integrating ML264 with LAG3-blocking monoclonal antibody relatlimab in GBM-bearing murine models. This synergistic strategy demonstrates significant preclinical potential for improving the treatment of recurrent GBM.

Our study identified the role of Gal3-LAG3 as the crucial regulator in maintaining exhaustion status of GBM-infiltrating T cells after recurrence. Furthermore, we dissected the molecular cascade mechanisms



(caption on next page)

**Fig. 6.** Radiotherapy combined with EGR1 inhibition and LAG3 blockade synergistically suppresses tumor progression and improves survival in GBM. A, Illustration of the in situ GBM model in immunocompromised mice and treatment with ML264 and/or Relatlimab after irradiation. B, Kaplan–Meier survival curves of NCG mice implanted with MES28 or 387 GSCs across different treatment groups, including vehicle control (DMSO), ML264, Relatlimab, and the combination of ML264 and Relatlimab, each with or without irradiation (IR) (n = 6 per group). C, *In vivo* bioluminescent imaging of tumor growth was performed in NCG mice bearing GBM xenografts derived from MES28 or 387 GSCs across different treatment groups, including vehicle control (DMSO), ML264, Relatlimab, and the combination of ML264 and Relatlimab, each with or without irradiation (IR), on days 1, 25, and 50 (n = 6 per group). D, Representative images of H&E staining of mouse brains collected on day 50, or at the onset of neurological symptoms, after transplantation of MES28 or 387 GSCs across different treatment groups, including vehicle control (DMSO), ML264, Relatlimab, and the combination of ML264 and Relatlimab, each with or without irradiation (IR). Scale bar, 2 mm (n = 6 per group). E–H, The mRNA expression of Gal3 in different glioma grades (II, III, and IV) from the CGGA, TCGA GBM LGG, Rembrandt and Gravendeel data sets. \*\*,  $P < .01$ . I–L, Kaplan–Meier survival analysis of Gal3 by the median of different glioma data sets: CGGA, TCGA, Rembrandt and Gravendeel GBM data sets.

governing Gal3 upregulation in recurrent GBM post-radiation, demonstrating that radiotherapy induces EGR1 expression in GSCs, which in turn activates Gal3 transcription in GSCs via direct promoter binding. Combined targeting of EGR1 in GSCs and LAG3 in T cells emerges as a rational strategy to reinvigorate exhausted T cells, thereby augmenting radiotherapy responses, mitigating GBM recurrence kinetics, and establishing a novel therapeutic axis for GBM intervention.

In line with prior reports that GSCs possess superior survival and adaptive capacities following radiotherapy and thereby contribute to GBM recurrence and treatment resistance, our work primarily focused on GSCs to elucidate mechanisms of therapeutic failure. Notably, while our study highlights GSCs as the predominant source of Gal3 following irradiation, we also found that Gal3 is expressed at appreciable levels in non-GSC tumor cells. This finding suggests that the functional influence of Gal3 may extend beyond GSCs, contributing more broadly to the immunosuppressive microenvironment of GBM. Further investigation into Gal3 expression and function in non-GSC tumor cells therefore represents an important avenue for future research.

Beyond Gal3 induction in GSCs, our analyses suggest that irradiation may also directly upregulate LAG3 expression on T cells. The enrichment of JAK/STAT3 and IL2/STAT5 signaling in recurrent GBM T cells, along with prior reports of radiation-induced immune checkpoint expression, supports this possibility. Such findings raise the hypothesis that radiation enhances T cell exhaustion via intrinsic STAT-mediated pathways, in parallel to Gal3-LAG3 interactions. The direct regulation of LAG3 in T cells following irradiation therefore represents an important direction for future investigation, requiring immune-focused single-cell analyses and functional validation. From a translational perspective, clarifying this dual mechanism, in which radiation simultaneously induces Gal3 expression in GSCs and upregulates LAG3 on T cells, may provide a more comprehensive understanding of immunosuppression in recurrent GBM. Future studies may inform the rational design of next-generation combination therapies that integrate radiotherapy with targeted inhibition of both tumor-intrinsic and T cell-intrinsic pathways [70]. Such an approach holds the potential to more effectively reverse T cell exhaustion, enhance radiotherapy responses, and ultimately improve patient outcomes.

In addition to Gal3, LAG3 binds several other ligands, including FGL1, CLEC4G, SNCA, and MHC class II molecules. Although our analyses indicate that these ligands are expressed at relatively low levels and lack strong prognostic relevance in GBM, their potential cooperative or context-dependent roles cannot be excluded. Future studies systematically investigating the interplay between multiple LAG3 ligands will be important to elucidate the complexity of LAG3-mediated immunoregulation and to inform more comprehensive therapeutic strategies.

#### CRedit authorship contribution statement

**Hui Huang:** Writing – review & editing, Writing – original draft, Visualization, Validation, Investigation, Funding acquisition, Data curation, Conceptualization. **Chenhua Li:** Writing – review & editing, Writing – original draft, Visualization, Validation, Methodology, Formal analysis, Data curation. **Hao You:** Writing – review & editing, Software,

Resources. **Zhen Zhang:** Writing – review & editing, Methodology, Investigation, Formal analysis. **Qiankun Lin:** Writing – review & editing, Supervision, Software, Resources. **Junlei Yang:** Writing – review & editing, Software, Resources. **Hang Yu:** Writing – review & editing, Resources, Investigation. **Zhiting Li:** Writing – review & editing, Project administration, Investigation. **Gaoyuan Cui:** Writing – review & editing, Resources, Methodology. **Kefan Song:** Writing – review & editing, Software, Resources. **Qian Zhang:** Writing – review & editing, Supervision, Resources. **Yun Chen:** Writing – review & editing, Supervision, Resources, Formal analysis. **Xiuxing Wang:** Writing – review & editing, Supervision, Resources, Project administration, Formal analysis, Conceptualization. **Junxia Zhang:** Writing – review & editing, Supervision, Resources. **Danling Gu:** Writing – review & editing, Writing – original draft, Supervision, Project administration, Formal analysis, Conceptualization. **Chao Cheng:** Writing – review & editing, Supervision, Project administration, Formal analysis. **Junfei Shao:** Writing – review & editing, Supervision, Resources, Funding acquisition, Formal analysis, Conceptualization.

#### Ethics approval and consent to participate

All patients' samples were collected from patients who gave informed consent, and all related procedures were performed with the approval of the internal review and ethics boards of the First Affiliated Hospital of Nanjing Medical University (2021-SR-076). Intracranial xenografts were established in 4–6-week-old female NCG mice under an animal protocol approved by the Institutional Animal Care and Use Committee (IACUC-2006033-2) at Nanjing Medical University in accordance with NIH and institutional guidelines.

#### Consent for publication

All authors approved the final manuscript and the submission to the journal.

#### Funding

This work was supported by the National Natural Science Foundation of China (82472670 to J.S., 82573133 to J.Z., and 82403427 to D.G.), China Postdoctoral Science Foundation (2023M741795 to D.G.), the Wuxi Taihu Lake Talent Plan - Supports for Leading Talents in Medical and Health Profession (2020THRC-DJ-SNW to J.S.), the Key Project of the Jiangsu Provincial Health Commission (ZD2022038 to J.S.) and 2024 Jiangsu Province Graduate Student Practice Program (SJCX24\_0728 to H.H.).

#### Declaration of competing interest

The authors declare the following financial interests/personal relationships which may be considered as potential competing interests: Junfei Shao reports financial support was provided by National Natural Science Foundation of China. Hui Huang reports financial support was provided by 2024 Jiangsu Province Graduate Student Practice Program.

Junfei Shao reports financial support was provided by Wuxi Taihu Lake Talent Plan - Supports for Leading Talents in Medical and Health Profession. Junfei Shao reports financial support was provided by Key Project of the Jiangsu Provincial Health Commission. If there are other authors, they declare that they have no known competing financial interests or personal relationships that could have appeared to influence the work reported in this paper.

## Acknowledgements

We thank the Nanjing Medical University Analysis Center for help with FACS, animal core facility of Nanjing Medical University for help with animal experiments.

## Appendix A. Supplementary data

Supplementary data to this article can be found online at <https://doi.org/10.1016/j.canlet.2025.218125>.

## Data availability

The RNA-sequencing data generated in this study are available in the GEO Database (GSE294744). All data accessed from external sources and prior publications have been referenced in the text and corresponding figure legends. Additional data used and/or analyzed during the current study are available from the corresponding author on reasonable request.

## References

- [1] L.R. Schaff, I.K. Mellinghoff, Glioblastoma and other primary brain malignancies in adults: a review, *JAMA* 329 (2023) 574–587.
- [2] C.M. Jackson, J. Choi, M. Lim, Mechanisms of immunotherapy resistance: lessons from glioblastoma, *Nat. Immunol.* 20 (2019) 1100–1109.
- [3] M. Weller, M. van den Bent, M. Preusser, E. Le Rhun, J.C. Tonn, G. Minniti, M. Bendzus, C. Balana, O. Chinot, L. Dirven, P. French, M.E. Hegi, A.S. Jakola, M. Platten, P. Roth, R. Ruda, S. Short, M. Smits, M.J.B. Taphoorn, A. von Deimling, M. Westphal, R. Soffietti, G. Reifenberger, W. Wick, EANO guidelines on the diagnosis and treatment of diffuse gliomas of adulthood, *Nat. Rev. Clin. Oncol.* 18 (2021) 170–186.
- [4] R. Stupp, M.E. Hegi, W.P. Mason, M.J. van den Bent, M.J. Taphoorn, R.C. Janzer, S. K. Ludwin, A. Allgeier, B. Fisher, K. Belanger, P. Hau, A.A. Brandes, J. Gijtenbeek, C. Marosi, C.J. Vecht, K. Mokhtari, P. Wesseling, S. Villa, E. Eisenhauer, T. Gorlia, M. Weller, D. Lacombe, J.G. Cairncross, R.O. Mirimanoff, R. European Organisation for, T. Treatment of Cancer Brain, G. Radiation Oncology, G. National Cancer Institute of Canada Clinical Trials, Effects of radiotherapy with concomitant and adjuvant temozolomide versus radiotherapy alone on survival in glioblastoma in a randomised phase III study: 5-year analysis of the EORTC-NCIC trial, *Lancet Oncol.* 10 (2009) 459–466.
- [5] R. Stupp, W.P. Mason, M.J. van den Bent, M. Weller, B. Fisher, M.J. Taphoorn, K. Belanger, A.A. Brandes, C. Marosi, U. Bogdahn, J. Curschmann, R.C. Janzer, S. K. Ludwin, T. Gorlia, A. Allgeier, D. Lacombe, J.G. Cairncross, E. Eisenhauer, R. O. Mirimanoff, R. European Organisation for, T. Treatment of Cancer Brain, G. Radiotherapy, G. National Cancer Institute of Canada Clinical Trials, Radiotherapy plus concomitant and adjuvant temozolomide for glioblastoma, *N. Engl. J. Med.* 352 (2005) 987–996.
- [6] M. Buehler, X. Yi, W. Ge, P. Blattmann, E. Rushing, G. Reifenberger, J. Felsberg, C. Yeh, J.E. Corn, L. Regli, J. Zhang, A. Cloos, V.M. Ravi, B. Wiestler, D.H. Heiland, R. Aebbersold, M. Weller, T. Guo, T. Weiss, Quantitative proteomic landscapes of primary and recurrent glioblastoma reveal a protumorigenic role for FBXO2-dependent glioma-microenvironment interactions, *Neuro Oncol.* 25 (2023) 290–302.
- [7] J.D. Lathia, S.C. Mack, E.E. Mulkearns-Hubert, C.L. Valentim, J.N. Rich, Cancer stem cells in glioblastoma, *Genes Dev.* 29 (2015) 1203–1217.
- [8] F. Sharifzad, S. Ghavami, J. Verdi, S. Mardpour, M. Mollapour Sisakht, Z. Azizi, A. Taghikhani, M.J. Los, E. Fakharian, M. Ebrahimi, A.A. Hamidieh, Glioblastoma cancer stem cell biology: potential therapeutic targets, *Drug Resist. Updates* 42 (2019) 35–45.
- [9] C.R. Goodwin, J. Laterra, Neuro-oncology: unmasking the multiforme in glioblastoma, *Nat. Rev. Neurol.* 6 (2010) 304–305.
- [10] S. Bao, Q. Wu, R.E. McLendon, Y. Hao, Q. Shi, A.B. Hjelmeland, M.W. Dewhirst, D. Bigner, J.N. Rich, Glioma stem cells promote radioresistance by preferential activation of the DNA damage response, *Nature* 444 (2006) 756–760.
- [11] J. Chen, Y. Li, T.S. Yu, R.M. McKay, D.K. Burns, S.G. Kernie, L.F. Parada, A restricted cell population propagates glioblastoma growth after chemotherapy, *Nature* 488 (2012) 522–526.
- [12] B.C. Prager, Q. Xie, S. Bao, J.N. Rich, Cancer Stem Cells, The architects of the tumor ecosystem, *Cell Stem Cell* 24 (2019) 41–53.
- [13] H. Lin, C. Liu, A. Hu, D. Zhang, H. Yang, Y. Mao, Understanding the immunosuppressive microenvironment of glioma: mechanistic insights and clinical perspectives, *J. Hematol. Oncol.* 17 (2024) 31.
- [14] S. Singh, D. Dey, D. Barik, I. Mohapatra, S. Kim, M. Sharma, S. Prasad, P. Wang, A. Singh, G. Singh, Glioblastoma at the crossroads: current understanding and future therapeutic horizons, *Signal Transduct. Targeted Ther.* 10 (2025) 213.
- [15] R. Sun, A.H. Kim, The multifaceted mechanisms of malignant glioblastoma progression and clinical implications, *Cancer Metastasis Rev.* 41 (2022) 871–898.
- [16] L. Zheng, S. Qin, W. Si, A. Wang, B. Xing, R. Gao, X. Ren, L. Wang, X. Wu, J. Zhang, N. Wu, N. Zhang, H. Zheng, H. Ouyang, K. Chen, Z. Bu, X. Hu, J. Ji, Z. Zhang, Pan-cancer single-cell landscape of tumor-infiltrating T cells, *Science* 374 (2021) abe6474.
- [17] X. Ren, L. Zhang, Y. Zhang, Z. Li, N. Siemers, Z. Zhang, Insights gained from single-cell analysis of immune cells in the tumor microenvironment, *Annu. Rev. Immunol.* 39 (2021) 583–609.
- [18] X. Zhou, F. Xie, L. Zhang, Tumor-immune cell interactions in cancer progression, *Cancer Res.* 85 (2025) 2963–2966.
- [19] Y. Aramaki, A. Kuroiwa, T. Nakamura, K. Ninomiya, Y. Fukuchi, T. Fukumoto, Y. Nakashima, Correlation of the size of isolated right ventricular infarction with the changes of ST segment in dogs, *Clin. Cardiol.* 10 (1987) 443–449.
- [20] C.U. Blank, W.N. Haining, W. Held, P.G. Hogan, A. Kallies, E. Lugli, R.C. Lynn, M. Philip, A. Rao, N.P. Restifo, A. Schietinger, T.N. Schumacher, P. L. Schwartzberg, A.H. Sharpe, D.E. Speiser, E.J. Wherry, B.A. Youngblood, D. Zehn, Defining 'T cell exhaustion', *Nat. Rev. Immunol.* 19 (2019) 665–674.
- [21] S.L. Topalian, P.M. Forde, L.A. Emens, M. Yarchoan, K.N. Smith, D.M. Pardoll, Neoadjuvant immune checkpoint blockade: a window of opportunity to advance cancer immunotherapy, *Cancer Cell* 41 (2023) 1551–1566.
- [22] V.A. Arrieta, C. Dmello, D.J. McGrail, D.J. Brat, C. Lee-Chang, A.B. Heimberger, D. Chand, R. Stupp, A.M. Sonabend, Immune checkpoint blockade in glioblastoma: from tumor heterogeneity to personalized treatment, *J. Clin. Investig.* 133 (2023).
- [23] M. Lim, Y. Xia, C. Bettgowda, M. Weller, Current state of immunotherapy for glioblastoma, *Nat. Rev. Clin. Oncol.* 15 (2018) 422–442.
- [24] W.J. Kelly, A.J. Giles, M. Gilbert, T lymphocyte-targeted immune checkpoint modulation in glioma, *J. Immunother. Cancer* 8 (2020).
- [25] D.F. Quail, J.A. Joyce, The microenvironmental landscape of brain tumors, *Cancer Cell* 31 (2017) 326–341.
- [26] A.R. Pombo Antunes, I. Scheyltjens, J. Duerinck, B. Neyns, K. Movahedi, J.A. Van Ginderachter, Understanding the glioblastoma immune microenvironment as basis for the development of new immunotherapeutic strategies, *eLife* 9 (2020).
- [27] B.M. Andersen, C. Faust Akl, M.A. Wheeler, E.A. Chiocca, D.A. Reardon, F. J. Quintana, Glial and myeloid heterogeneity in the brain tumour microenvironment, *Nat. Rev. Cancer* 21 (2021) 786–802.
- [28] L. Cai, Y. Li, J. Tan, L. Xu, Y. Li, Targeting LAG-3, TIM-3, and TIGIT for cancer immunotherapy, *J. Hematol. Oncol.* 16 (2023) 101.
- [29] Z. Zhang, L. Chen, H. Chen, J. Zhao, K. Li, J. Sun, M. Zhou, Pan-cancer landscape of T-cell exhaustion heterogeneity within the tumor microenvironment revealed a progressive roadmap of hierarchical dysfunction associated with prognosis and therapeutic efficacy, *EBioMedicine* 83 (2022) 104207.
- [30] X. Wang, K. Yang, Q. Xie, Q. Wu, S.C. Mack, Y. Shi, L.J.Y. Kim, B.C. Prager, W. A. Flavahan, X. Liu, M. Singer, C.G. Hubert, T.E. Miller, W. Zhou, Z. Huang, X. Fang, A. Regev, M.L. Suva, T.H. Hwang, J.W. Locasale, S. Bao, J.N. Rich, Purine synthesis promotes maintenance of brain tumor initiating cells in glioma, *Nat. Neurosci.* 20 (2017) 661–673.
- [31] X. Wang, Z. Huang, Q. Wu, B.C. Prager, S.C. Mack, K. Yang, L.J.Y. Kim, R. C. Gimple, Y. Shi, S. Lai, Q. Xie, T.E. Miller, C.G. Hubert, A. Song, Z. Dong, W. Zhou, X. Fang, Z. Zhu, V. Mahadev, S. Bao, J.N. Rich, MYC-regulated mevalonate metabolism maintains brain tumor-initiating cells, *Cancer Res.* 77 (2017) 4947–4960.
- [32] X. Wang, K. Yang, Q. Wu, L.J.Y. Kim, A.R. Morton, R.C. Gimple, B.C. Prager, Y. Shi, W. Zhou, S. Bhargava, Z. Zhu, L. Jiang, W. Tao, Z. Qiu, L. Zhao, G. Zhang, X. Li, S. Agnihotri, P.S. Mischel, S.C. Mack, S. Bao, J.N. Rich, Targeting pyrimidine synthesis accentuates molecular therapy response in glioblastoma stem cells, *Sci. Transl. Med.* 11 (2019).
- [33] D. Dixit, B.C. Prager, R.C. Gimple, H.X. Poh, Y. Wang, Q. Wu, Z. Qiu, R.L. Kidwell, L.J.Y. Kim, Q. Xie, K. Vitting-Seerup, S. Bhargava, Z. Dong, L. Jiang, Z. Zhu, P. Hamerlik, S.R. Jaffrey, J.C. Zhao, X. Wang, J.N. Rich, The RNA m6A reader YTHDF2 maintains oncogene expression and is a targetable dependency in glioblastoma stem cells, *Cancer Discov.* 11 (2021) 480–499.
- [34] J. Gao, D. Gu, K. Yang, J. Zhang, Q. Lin, W. Yuan, X. Zhu, D. Dixit, R.C. Gimple, H. You, Q. Zhang, Z. Shi, X. Fan, Q. Wu, C. Lu, Z. Cheng, D. Li, L. Zhao, B. Xue, Z. Zhu, Z. Zhu, H. Yang, N. Zhao, W. Gao, Y. Lu, J. Shao, C. Cheng, D. Hao, S. Yang, Y. Chen, X. Wang, C. Kang, J. Ji, J. Man, S. Agnihotri, Q. Wang, F. Lin, X. Qian, S. C. Mack, Z. Hu, C. Li, M.D. Taylor, Y. Li, N. Zhang, J.N. Rich, Y. You, X. Wang, Infiltrating plasma cells maintain glioblastoma stem cells through IgG-Tumor binding, *Cancer Cell* 43 (2025) 122–143 e128.
- [35] J. Zhong, X. Yang, J. Chen, K. He, X. Gao, X. Wu, M. Zhang, H. Zhou, F. Xiao, L. An, X. Wang, Y. Shi, N. Zhang, Circular EZH2-encoded EZH2-92aa mediates immune evasion in glioblastoma via inhibition of surface NKG2D ligands, *Nat. Commun.* 13 (2022) 4795.
- [36] L. Sun, Y. Su, A. Jiao, X. Wang, B. Zhang, T cells in health and disease, *Signal Transduct. Targeted Ther.* 8 (2023) 235.
- [37] A.C. Anderson, N. Joller, V.K. Kuchroo, Lag-3, Tim-3, and TIGIT: Co-inhibitory receptors with specialized functions in immune regulation, *Immunity* 44 (2016) 989–1004.

- [38] D. Lv, R.C. Gimple, C. Zhong, Q. Wu, K. Yang, B.C. Prager, B. Godugu, Z. Qiu, L. Zhao, G. Zhang, D. Dixit, D. Lee, J.Z. Shen, X. Li, Q. Xie, X. Wang, S. Agnihotri, J. N. Rich, PDGF signaling inhibits mitophagy in glioblastoma stem cells through N (6)-methyladenosine, *Dev. Cell* 57 (2022) 1466–1481 e1466.
- [39] A. Ruiz de Sabando, C. Wang, Y. He, M. Garcia-Barros, J. Kim, K.R. Shroyer, T. D. Bannister, V.W. Yang, A.B. Bialkowska MI264, A novel small-molecule compound that potentially inhibits growth of colorectal cancer, *Mol. Cancer Therapeut.* 15 (2016) 72–83.
- [40] Y. Wang, Y. Cui, J. Liu, Q. Song, M. Cao, Y. Hou, X. Zhang, P. Wang, Kruppel-like factor 5 accelerates the pathogenesis of Alzheimer's disease via BACE1-mediated APP processing, *Alzheimers Res. Ther.* 14 (2022) 103.
- [41] H.A. Tawbi, D. Schadendorf, E.J. Lipson, P.A. Ascierto, L. Matamala, E. Castillo Gutierrez, P. Rutkowski, H.J. Gogas, C.D. Lao, J.J. De Menezes, S. Dalle, A. Arance, J.J. Grob, S. Srivastava, M. Abaskharoun, M. Hamilton, S. Keidel, K.L. Simonsen, A. M. Sobieski, B. Li, F.S. Hodi, G.V. Long, R.- Investigators, Relatlimab and Nivolumab versus Nivolumab in untreated advanced melanoma, *N. Engl. J. Med.* 386 (2022) 24–34.
- [42] R.C. Gimple, S. Bhargava, D. Dixit, J.N. Rich, Glioblastoma stem cells: lessons from the tumor hierarchy in a lethal cancer, *Genes Dev.* 33 (2019) 591–609.
- [43] Q. Weng, J. Wang, J. Wang, D. He, Z. Cheng, F. Zhang, R. Verma, L. Xu, X. Dong, Y. Liao, X. He, A. Potter, L. Zhang, C. Zhao, M. Xin, Q. Zhou, B.J. Aronow, P. J. Blackshear, J.N. Rich, Q. He, W. Zhou, M.L. Suva, R.R. Wacław, S.S. Potter, G. Yu, Q.R. Lu, Single-cell transcriptomics uncovers glial progenitor diversity and cell fate determinants during development and gliomagenesis, *Cell Stem Cell* 24 (2019) 707–723 e708.
- [44] A.G. Alvarado, P.S. Thiagarajan, E.E. Mulkearns-Hubert, D.J. Silver, J.S. Hale, T. J. Alban, S.M. Turaga, A. Jarrar, O. Reizes, M.S. Longworth, M.A. Vogelbaum, J. D. Lathia, Glioblastoma cancer stem cells evade innate immune suppression of self-renewal through reduced TLR4 expression, *Cell Stem Cell* 20 (2017) 450–461 e454.
- [45] Z. Qiu, L. Zhao, J.Z. Shen, Z. Liang, Q. Wu, K. Yang, L. Min, R.C. Gimple, Q. Yang, S. Bhargava, C. Jin, C. Kim, D. Hinz, D. Dixit, J.A. Bernatchez, B.C. Prager, G. Zhang, Z. Dong, D. Lv, X. Wang, L.J.Y. Kim, Z. Zhu, K.A. Jones, Y. Zheng, X. Wang, J.L. Siqueira-Neto, L. Chavez, X.D. Fu, C. Spruck, J.N. Rich, Transcription elongation machinery is a druggable dependency and potentiates immunotherapy in glioblastoma stem cells, *Cancer Discov.* 12 (2022) 502–521.
- [46] H. Yuan, X. Wu, Q. Wu, A. Chatoff, E. Megill, J. Gao, T. Huang, T. Duan, K. Yang, C. Jin, F. Yuan, S. Wang, L. Zhao, P.O. Zinn, K.G. Abdullah, Y. Zhao, N.W. Snyder, J.N. Rich, Lysine catabolism reprograms tumour immunity through histone crotonylation, *Nature* 617 (2023) 818–826.
- [47] P.K. Bommarreddy, H. Wakimoto, R.L. Martuza, H.L. Kaufman, S.D. Rabkin, D. Saha, Oncolytic herpes simplex virus expressing IL-2 controls glioblastoma growth and improves survival, *J. Immunother.* Cancer 12 (2024).
- [48] H. Sadahiro, K.D. Kang, J.T. Gibson, M. Minata, H. Yu, J. Shi, R. Chhipa, Z. Chen, S. Lu, Y. Simoni, T. Furuta, H. Sabit, S. Zhang, S. Bastola, S. Yamaguchi, H. Alsheikh, S. Komarova, J. Wang, S.H. Kim, D. Hambardzumyan, G. Lu, E. W. Newell, B. DasGupta, M. Nakada, L.J. Lee, B. Nabors, L.A. Norian, I. Nakano, Activation of the receptor tyrosine kinase AXL regulates the immune microenvironment in glioblastoma, *Cancer Res.* 78 (2018) 3002–3013.
- [49] E. Bouffet, V. Larouche, B.B. Campbell, D. Merico, R. de Borja, M. Aronson, C. Durno, J. Krueger, V. Cabric, V. Ramaswamy, N. Zhukova, G. Mason, R. Farah, S. Afzal, M. Yalon, G. Rechavi, V. Magimairajan, M.F. Walsh, S. Constantini, R. Dvir, R. Elhasid, A. Reddy, M. Osborn, M. Sullivan, J. Hansford, A. Dodgshun, N. Klauber-Demore, L. Peterson, S. Patel, S. Lindhorst, J. Atkinson, Z. Cohen, R. Laframboise, P. Dirks, M. Taylor, D. Malkin, S. Albrecht, R.W. Dudley, N. Jabado, C.E. Hawkins, A. Shlien, U. Tabori, Immune checkpoint inhibition for hypermutant glioblastoma multiforme resulting from germline Biallelic mismatch repair deficiency, *J. Clin. Oncol.* 34 (2016) 2206–2211.
- [50] T.M. Johannis, C.A. Miller, I.G. Dordward, C. Tsien, E. Chang, A. Perry, R. Uppaluri, C. Ferguson, R.E. Schmidt, S. Dahiya, G. Ansstas, E.R. Mardis, G.P. Dunn, Immunogenomics of hypermutated glioblastoma: a patient with germline POLE deficiency treated with checkpoint blockade immunotherapy, *Cancer Discov.* 6 (2016) 1230–1236.
- [51] D.A. Reardon, A.A. Brandes, A. Omuro, P. Mulholland, M. Lim, A. Wick, J. Baehring, M.S. Ahluwalia, P. Roth, O. Bahr, S. Phuphanich, J.M. Sepulveda, P. De Souza, S. Sahebjam, M. Carleton, K. Tatsuoka, C. Tait, R. Zwierts, J. Sampson, M. Weller, Effect of Nivolumab vs Bevacizumab in patients with recurrent glioblastoma: the CheckMate 143 phase 3 randomized clinical trial, *JAMA Oncol.* 6 (2020) 1003–1010.
- [52] L. Chocarro, E. Blanco, M. Zuazo, H. Arasanz, A. Bocanegra, L. Fernandez-Rubio, P. Morente, G. Fernandez-Hinojal, M. Echaide, M. Garnica, P. Ramos, R. Vera, G. Kochan, D. Escors, Understanding LAG-3 signaling, *Int. J. Mol. Sci.* 22 (2021).
- [53] S. Grebinoski, Q. Zhang, A.R. Cillo, S. Manne, H. Xiao, E.A. Brunazzi, T. Tabib, C. Cardello, C.G. Lian, G.F. Murphy, R. Lafyatis, E.J. Wherry, J. Das, C.J. Workman, D.A.A. Vignali, Autoreactive CD8(+) T cells are restrained by an exhaustion-like program that is maintained by LAG3, *Nat. Immunol.* 23 (2022) 868–877.
- [54] S. Yuan, N.S. Fuchs, S.A. Abdel-Rahman, B. Kaur, M.T. Gabr, TREM2 and LAG-3 in cancer and Alzheimer's disease immunotherapy, *Trends Pharmacol. Sci.* 46 (2025) 738–751.
- [55] J. Wang, C. Klein, J.R. Cochran, J. Sockolosky, S.M. Lippow, Exploring new frontiers in LAG-3 biology and therapeutics, *Trends Pharmacol. Sci.* 46 (2025) 638–652.
- [56] R. Li, J. Qiu, Z. Zhang, C. Qu, Z. Tang, W. Yu, Y. Tian, H. Tian, Prognostic significance of Lymphocyte-activation gene 3 (LAG3) in patients with solid tumors: a systematic review, meta-analysis and pan-cancer analysis, *Cancer Cell Int.* 23 (2023) 306.
- [57] O. Hamid, K.D. Lewis, A. Weise, M. McKean, K.P. Papadopoulos, J. Crown, T. M. Kim, D.H. Lee, S.S. Thomas, J. Mehnert, J. Kaczmar, N.J. Lakhani, K.B. Kim, M. R. Middleton, G. Rabinowits, A.I. Spira, M. Yushak, I. Mehmi, F. Fang, S. Chen, J. Mani, V. Jankovic, F. Wang, N. Fiaschi, L. Brennan, A. Paccaly, S. Masinde, M. Salvati, M.G. Fury, G. Kroog, I. Lowy, G. Gullo, Phase I study of fiantlimab, a human lymphocyte activation Gene-3 (LAG-3) monoclonal antibody, in combination with cemiplimab in advanced melanoma, *J. Clin. Oncol.* 42 (2024) 2928–2938.
- [58] E. Garralda, A. Sukari, N.J. Lakhani, A. Patnaik, Y. Lou, S.A. Im, T. Golan, R. Geva, M. Wermke, M. de Miguel, J. Palcza, S. Jha, M. Chaney, A.K. Abraham, J. Healy, G. S. Falchook, A first-in-human study of the anti-LAG-3 antibody favezelimab plus pembrolizumab in previously treated, advanced microsatellite stable colorectal cancer, *ESMO Open* 7 (2022) 100639.
- [59] D. Davar, A.C. Anderson, I. Diaz-Padilla, Therapeutic potential of targeting LAG-3 in cancer, *J. Immunother. Cancer* 13 (2025).
- [60] Y.G. Wang, S.J. Kim, J.H. Baek, H.W. Lee, S.Y. Jeong, K.H. Chun, Galectin-3 increases the motility of mouse melanoma cells by regulating matrix metalloproteinase-1 expression, *Exp. Mol. Med.* 44 (2012) 387–393.
- [61] I.Y. Zhang, S. Liu, L. Zhang, R. Liang, Q. Fang, J. Zhao, L. Ren, E.F. Medina, A. Filippov, K.J. Bonjoc, A. Chaudhry, M. Dayyani, A.H. Bild, B. Badie, RAGE ablation attenuates glioma progression and enhances tumor immune responses by suppressing galectin-3 expression, *Neuro Oncol.* 25 (2023) 886–898.
- [62] M. Farhad, A.S. Rolig, W.L. Redmond, The role of Galectin-3 in modulating tumor growth and immunosuppression within the tumor microenvironment, *Oncolimmunology* 7 (2018) e1434467.
- [63] A. Chen, Y. Jiang, Z. Li, L. Wu, U. Santiago, H. Zou, C. Cai, V. Sharma, Y. Guan, L. H. McCarl, J. Ma, Y.L. Wu, J. Michel, Y. Shi, L. Konnikova, N.M. Amankulor, P. O. Zinn, G. Kohanbash, S. Agnihotri, S. Lu, X. Lu, D. Sun, G.K. Gittes, Q. Wang, X. Xiao, D. Yimlamai, I.F. Pollack, C.J. Camacho, B. Hu, Chitinase-3-like 1 protein complexes modulate macrophage-mediated immune suppression in glioblastoma, *J. Clin. Invest.* 131 (2021).
- [64] Q. Jiang, Q. Zhao, Y. Chen, C. Ma, X. Peng, X. Wu, X. Liu, R. Wang, S. Hou, L. Kong, Y. Wan, S. Wang, Z.X. Meng, B. Cui, L. Chen, P. Li, Galectin-3 impairs calcium transients and beta-cell function, *Nat. Commun.* 15 (2024) 3682.
- [65] S.M. Melief, M. Visser, S.H. van der Burg, E.M.E. Verdegaal, IDO and galectin-3 hamper the ex vivo generation of clinical grade tumor-specific T cells for adoptive cell therapy in metastatic melanoma, *Cancer Immunol. Immunother.* 66 (2017) 913–926.
- [66] Y. Fan, S. Song, Y. Li, S.S. Dhar, J. Jin, K. Yoshimura, X. Yao, R. Wang, A.W. Scott, M.P. Pizzi, J. Wu, L. Ma, G.A. Calin, S. Hanash, L. Wang, M. Curran, J.A. Ajani, Galectin-3 cooperates with CD47 to suppress phagocytosis and T-cell immunity in gastric cancer peritoneal metastases, *Cancer Res.* 83 (2023) 3726–3738.
- [67] R.C. Gilson, S.D. Gunasinghe, L. Johannes, K. Gaus, Galectin-3 modulation of T-cell activation: mechanisms of membrane remodelling, *Prog. Lipid Res.* 76 (2019) 101010.
- [68] X. Shen, Y. Zhang, Z. Xu, H. Gao, W. Feng, W. Li, Y. Miao, Z. Xu, Y. Zong, J. Zhao, A. Lu, KLF5 inhibition overcomes oxaliplatin resistance in patient-derived colorectal cancer organoids by restoring apoptotic response, *Cell Death Dis.* 13 (2022) 303.
- [69] J. Kim, C. Wang, A.R. de Sabando, H.L. Cole, T.J. Huang, J. Yang, T.D. Bannister, V. W. Yang, A.B. Bialkowska, The novel small-molecule SR18662 efficiently inhibits the growth of colorectal cancer in vitro and in vivo, *Mol. Cancer Therapeut.* 18 (2019) 1973–1984.
- [70] L. Galluzzi, M.J. Aryankalayil, C.N. Coleman, S.C. Formenti, Emerging evidence for adapting radiotherapy to immunotherapy, *Nat. Rev. Clin. Oncol.* 20 (2023) 543–557.